Contrib Mineral Petrol (2004) 146: 414–432
DOI 10.1007/s00410-003-0511-9

ORIGINAL PAPER

Jürgen Koepke · Sandrin T. Feig · Jonathan Snow
Marcus Freise

Petrogenesis of oceanic plagiogranites by partial melting of gabbros: an experimental study

Received: 25 April 2003 / Accepted: 8 August 2003 / Published online: 9 September 2003

Abstract We performed hydrous partial melting experiments at shallow pressures (0.2 GPa) under slightly oxidizing conditions (NNO oxygen buffer) on oceanic cumulate gabbros drilled by ODP (Ocean Drilling Program) cruises to evaluate whether the partial melting of oceanic gabbro can generate SiO_2-rich melts with compositions typical of oceanic plagiogranites. The experimental melts of the low-temperature runs broadly overlap those of natural plagiogranites. At 940 °C, the normalized SiO_2 contents of the experimental melts of all systems range between 60 and 61 wt%, and at 900 °C between 63 and 68 wt%. These liquids are characterized by low TiO_2 and FeO^{tot} contents, similar to those of natural plagiogranites from the plutonic section of the oceanic crust, but in contrast to Fe and Ti-rich low-temperature experimental melts obtained in MORB systems at ~950 °C. The ~1,500-m-long drilled gabbroic section of ODP Hole 735B (Legs 118 and 176) at the Southwest Indian Ridge contains numerous small plagiogranitic veins often associated with zones which are characterized by high-temperature shearing. The compositions of the experimental melts obtained at low temperatures match those of the natural plagiogranitic veins, while the compositions of the crystals of low-temperature runs correspond to those of minerals from high-temperature microscopic veins occurring in the gabbroic section of the Hole 735B. This suggests that the observed plagiogranitic veins are products of a partial melting process triggered by a water-rich fluid phase. If the temperature estimations for high-temperature shear zones are correct (up to 1,000 °C), and a water-rich fluid phase is present, the formation of plagiogranites by partial melting of gabbros is probably a widespread phenomenon in the genesis of the ocean crust.

Editorial responsibility: J. Hoefs

J. Koepke (✉) · S. T. Feig · M. Freise
Institut für Mineralogie, Universität Hannover,
Welfengarten 1, 30167, Hannover, Germany
E-mail: koepke@mineralogie.uni-hannover.de
Tel.: +49-0511-7624084
Fax: +49-0511-7623045

J. Snow
Max-Planck-Institute for Chemistry,
Postfach 3060, 55020 Mainz, Germany

Introduction

Layer 3 of the oceanic crust largely consists of gabbroic rocks. Included in the gabbroic section are small, but ubiquitous, amounts of felsic, evolved rocks including diorites, quartz diorites, tonalites, trondjhemites, so-called oceanic plagiogranites (Thayer 1977; Coleman and Donato 1979; Aldiss 1981). Such rocks were drilled in several ODP (Ocean Drilling Program) locations: Southwest Indian Ridge (SWIR), Leg 118 (Hébert et al. 1991) and Leg 176 (Dick et al. 2000); Mid-Atlantic Ridge, Leg 153 (Casey 1997) and are also present in the plutonic sections of most ophiolites (e.g., Nicolas 1989). For their genesis, two different models are under discussion: (1) extreme differentiation of a MORB-related source; and (2) partial melting of pre-existing gabbros within high-temperature shear zones.

1. For the confirmation of the first model, numerous experimental studies have been carried out by a number of investigators, mainly at 1 atm in the dry system. These works show that the generation of SiO_2-rich melts is possible via the fractionation of Fe-Ti oxides during late stage differentiation of a tholeiitic melt (e.g., Juster et al. 1989; Shi 1993; Thy and Lofgren 1994; Toplis and Carroll 1995). Dixon-Spulber and Rutherford (1983) verified the generation of plagiogranitic melts in hydrous MORB systems by performing partial melting experiments on MORB basalts at pressures between 100 and 300 MPa and low oxygen fugacity (fO_2). Recently, Berndt (2002) showed via crystallization experiments on hydrous MORB glasses that the experimental melts at the lowest run temperature (950 °C) at

different water contents and oxygen fugacities show plagiogranitic compositions (SiO_2 content of 60–64; K_2O < 0.5 wt%).

2. The second model for the generation of SiO_2-rich rocks within the oceanic crust is the partial melting of gabbroic rocks in tectonically active areas of mid-ocean ridge systems. Examples for this are described from ophiolite sections exclusively (see next section). Their occurrence is spatially related to high-temperature shear zones observed in these ophiolites. Meanwhile, high-temperature shear zones within the gabbroic section of the oceanic crust have been observed by several ODP drilling legs: SWIR–Legs 118, 176 (Dick et al. 2000); Mid-Atlantic Ridge (MARK area)–Leg 153 (Cortesogno et al. 2000); East Pacific Rise (Hess Deep)–Leg 147 (Früh-Green et al. 1996); Iberia Abyssal Plain–Leg 149 (Seifert et al. 1996). Here, metamorphosed, often ductilely sheared gabbros occur at metamorphic grades from greenschist to granulite facies. For some granulite-facies metagabbros from the SWIR (Dick et al. 2000) and Mid-Atlantic Ridge (Cortesogno et al. 2000), typical "magmatic" conditions were estimated with temperatures up to 1,000 °C at pressures between 100 and 300 MPa. At such conditions, gabbroic rocks could generate partial melts, provided a water-rich volatile phase is present. The role of water in generating plagiogranitic melts is suggested by the common presence of amphibole in felsic rocks of the oceanic crust (e.g., Coleman 1977; Aldiss 1981; Nicolas 1989; Bébien 1991; Floyd et al. 1998; Beard 1998; Tsikouras and Hatzipanagiotou 1998; Koepke et al. 2002), pointing towards elevated water activities in the corresponding melts. Amphiboles in plagiogranites often show poikilitic textures with inclusions of plagioclase and sometimes clinopyroxene, clearly indicating a magmatic origin (e.g., Koepke 1986). Up to now, an experimental investigation of this phenomenon has been lacking. It is the aim of this paper to address, experimentally, whether or not partial melting of oceanic gabbro has the potential for the generation of plagiogranitic melts. Therefore, we performed melting experiments on three typical gabbros from ODP Legs 176 (SWIR) and 153 (Mid-Atlantic Ridge). It should be noted that oceanic gabbros show a marked refractory character in composition (high contents of MgO and Al_2O_3, low contents in incompatible elements), which is in contrast to the composition of tholeiite basalts used in the experimental studies mentioned above.

The redox conditions of the potential melting processes within the oceanic crust are presently not well constrained. The fO_2 for typical, primitive MORB melts are varying between QFM (quartz-fayalite-magnetite buffer) to QFM-1 (Christie et al. 1986). These melts are assumed to be relatively dry (see below), and any increase of aH_20 will have an oxidizing effect (e.g., Scaillet et al. 1995; Berndt 2002). Since our melting experiments were conducted under water-saturation, we have chosen slightly oxidizing conditions for our experiments at fO_2 corresponding to the NNO oxygen buffer (Ni-NiO; ~QFM +1), which is 1–2 log-units above those values for primitive MORB melts. Since the potential locations for partial melting events within the deep oceanic crust (the high-temperature shear zones) are also pathways for hydrothermal circulation causing alteration processes, it is reasonable to assume that the redox conditions in high-temperature shear zones are more oxidizing than reducing.

Natural examples of oceanic plagiogranites formed by partial melting

Most plagiogranites assumed to be generated by partial melting of pre-existing basic rocks are reported from ophiolites, mainly based on trace element geochemistry (Malpas 1979; Gerlach et al. 1981; Pedersen and Malpas 1984; Spray and Dunning 1991; Flagler and Spray 1991; Bédard 1991; Amri et al. 1996). In some cases, field relations and textural observations suggest that anatexis was coeval to high-temperature shearing (Malpas 1979; Pedersen and Malpas 1984; Spray and Dunning 1991; Flagler and Spray 1991). Mével (1988) also reports occurrences of anatexis in young oceanic crust.

A fundamental problem concerning the previous work is that a precise characterization of the potential basic protolith is lacking. Possible candidates for protoliths located in the lower or middle oceanic crust may be cumulate gabbros, high-level gabbros, oxide gabbros, sheeted dikes (corresponding to MORB-type basalts), or any mixtures of these rocks. In addition, these rocks may exist in a fresh state, or they may be more or less hydrated or hydrothermally altered, or even influenced by seawater-derived fluids, leading to a broad range in potential protolith compositions. Since the compositions of the liquids generated by partial melting are sensitive to the composition of the protolith (for details see examples in Johannes and Holtz 1996 and references therein), it is difficult to predict the composition of a potential partial melt without a detailed knowledge of the composition of the protolith, even if the parameters of the melting reaction (e.g., temperature, aH_2O) are known. The attempt of the present paper is the quantification of such partial melting processes by using three different types of oceanic gabbros as source material for partial melting experiments.

Previous experiments on partial melting of basic rocks

Our understanding of the partial melting of basic rocks has grown significantly over the last two decades, since numerous experimental studies on dehydration melting

of amphibolites have been performed (e.g., Hacker 1990; Beard and Lofgren 1991; Rapp et al. 1991; Rushmer 1991, 1993; Sen and Dunn 1994; Wolf and Wyllie 1994; Rapp and Watson 1995; Patino Douce and Beard 1995; Johannes and Koepke 2001). The aim of these works was to investigate, experimentally, the genesis of the Archean tonalites, trondhjemites, and granodiorites (TTG rocks; Barker 1979) by dehydration melting of amphibolites or greenstones. Furthermore, a few experimental papers dealt with the partial melting of basalts under hydrous conditions (Holloway and Burnham 1972; Helz 1973; Beard and Lofgren 1991; Kawamoto 1996). In general, these papers show that partial melting of basic rocks could produce silicic melts. Recently, Koepke et al. (2003) investigated the partial melting behavior of an ocean-island type ferrogabbro at shallow pressures. The experimental melt generated at the lowest temperature (930 °C) show too low of a SiO_2 content and too high an amount of K_2O when comparing with typical natural oceanic plagiogranite.

However, the results of the papers mentioned above cannot be applied directly to the genesis of plagiogranites by partial melting of oceanic gabbros under shallow pressures. Firstly, the composition of the starting materials of those studies (e.g., Archean tholeiite, quartz tholeiite, alkali basalt, high-alumina basalt, ferrogabbro) differ markedly from those of typical oceanic gabbros, which are much more depleted in incompatible elements. Secondly, the experimental pressures of most of the dehydration melting studies mentioned above are distinctly higher (in general ≥500 MPa) than those relevant for the high-temperature shearing processes in the ocean crust (100–200 MPa). This typically results in the presence of garnet in the experimental crystal assemblages (e.g., Johannes and Koepke 2001); a feature unknown in the oceanic crust.

Experimental and analytical techniques

Starting materials

Rock powders of three natural gabbros were used as starting material for the melting experiments. The compositions are listed in Table 1. The minerals were examined by the electron microprobe and found to be homogeneous, showing only slight zoning. Two samples are from ODP Leg 176 at SWIR, where an exceptionally long section of the gabbroic layer was drilled with a total length of 1,508 m (hole 735B, together with Leg 118, Dick et al. 2000).

Sample 61a (176–735B-166R-2:61–71) is a coarse-grained olivine clinopyroxene gabbro, with modal proportion of plagioclase (An_{55}), olivine (Fo_{61}), and clinopyroxene [Mg# = 78; molar 100×MgO/(MgO + FeO)] of ~50:25:25 (vol%). Secondary accessory minerals include amphibole, oxides, and sulfides. The rock shows only very limited signs of alteration, mainly related to the formation of tiny films of serpentine along fractures in olivine.

Sample 101 (176–735B-91R-2:101–110) is a coarse-grained olivine gabbro containing plagioclase (An_{69}), olivine (Fo_{77}), and clinopyroxene (Mg# = 84) in the proportions ~50:40:10. This rock is somewhat altered which is expressed by coronas around olivine and clinopyroxene consisting mainly of serpentine, sometimes accompanied by tiny grains of oxides and sulfides. Plagioclase is generally slightly clouded indicating initial alteration.

The sample 923A (153–923A-2R-2:74–82) is from Leg 153 from the MARK area of the Mid-Atlantic ridge (provided by Laura Gaggero, Genova, Italy), where many of the drilled gabbros showed signs of intense plastic deformation (Gaggero and Cortesogno 1997; Cortesogno et al. 2000). This coarse-grained rock shows a gneissic texture with elongated plagioclase (An_{53}), olivine (Fo_{66}), clinopyroxene (Mg# = 75) in the proportions ~50:20:30. The rock contains a few percent of titanian pargasite rimming clinopyroxene and filling interstices.

Rock chips were milled using a mortar mill to a grain size from < 1 to > 50 μm. To minimize the presence of relics of the starting minerals in our experiments, the rock powder was classified into charges of different grain sizes with the help of the Atterberg sedimentation method. We used the powder fraction 2–10 μm as starting material for the melting experiments.

Previous experiments on hydrous silicate melts have shown that the presence of amphibole requires melt water contents of 4 to 5 wt% (Merzbacher and Eggler 1984; Johnson et al. 1994). Accordingly, we added a constant amount of water to the starting material so that water-saturated conditions were attained in our runs. To determine the influence of water on the phase relations and compositions, a few runs with reduced water activities were also performed.

Experimental techniques

The melting experiments were performed in an internally heated pressure vessel (IHPV) pressured with argon at 200 MPa and in the temperature interval between 900 and 1,060 °C. Pressure was measured with a strain gauge manometer with an uncertainty of ± 50 bar. Variation in T over the sample was less than 10 °C in all experiments and temperature is believed to be accurate within ± 10 °C. After the run, the samples were quenched isobarically with the help of a rapid quench facility to avoid the formation of quench crystals during cooling. fO_2 in our runs were controlled by setting a distinct partial pressure of hydrogen, which was controlled with the help of a membrane made of Pt (“Shaw membrane”). Details of the IHPV used are reported in Berndt et al. (2002). The fO_2 of our water-saturated runs corresponds in general to the NNO buffer. Water-saturation was achieved by adding 10% water to the charge. Only at one temperature (980 °C, sample 61a) runs with reduced water activities were performed by adding mixtures of water and silver oxalate leading to a XH_2O in the fluid phase of 0.8, 0.6, and 0.4 (initial loaded fluid phase composition;

Table 1 Chemical compositions of the starting gabbros: grain size fraction 2–10 μm

Sample	n^a	SiO_2	TiO_2	Al_2O_3	FeO^{tot}	MnO	MgO	CaO	Na_2O	K_2O	Total
61a	7	52.15 (0.24)	0.36 (0.02)	17.71 (0.13)	4.77 (0.22)	0.11 (0.07)	9.10 (0.12)	11.66 (0.17)	3.15 (0.14)	0.07 (0.02)	99.09
101	8	47.00 (0.33)	0.15 (0.03)	18.84 (0.08)	7.18 (0.27)	0.14 (0.06)	15.05 (0.15)	8.46 (0.19)	2.07 (0.19)	0.31 (0.03)	99.19
923A	9	51.79 (0.17)	0.27 (0.03)	17.02 (0.18)	6.80 (0.23)	0.10 (0.06)	10.96 (0.11)	9.29 (0.08)	2.95 (0.18)	0.09 (0.02)	99.28

Averages of electron microprobe analyses of glasses synthesized by fusing the rock powders of the starting gabbros
ODP sample descriptions: 61a: 176–735B–166R–2:61–71; 101:176–735B–91R–2:101–110; 923A: 153–923A–2R–2:74–82
[a]Number of analyses; the number in parentheses corresponds to the standard deviation

$XH_2O = XH_2O/(XH_2O + XCO_2)$, in moles). In these runs, the fO_2 was somewhat lower than NNO, since in an oxygen buffered system using H_2 as fO_2 constraining medium, the fO_2 depends on aH_2O. In those runs with $aH_2O < 1$ the fO_2 varied between the QFM and NNO buffer as a function of aH_2O.

For the runs at temperatures < 1,060 °C, Au was used as capsule material. To minimize iron loss in runs at temperatures of 1,060 °C, capsules made of $Au_{80}Pd_{20}$ pre-saturated with iron were used (for details see Berndt 2002). To check a potential iron-loss, Fe-microprobe traverses were measured through larger melt pools of the middle and of the rim of the samples and, in addition, through the adjacent container wall. No evidence of iron loss was detected.

Analytical method

The analyses of the experimental phases were performed with a Cameca SX100 electron microprobe equipped with five spectrometers and an operating system "Peak sight" based on Microsoft Windows 2000. All data were obtained using 15 kV acceleration potential, a static (fixed) beam, Kα emission from all elements, and a matrix correction according to Pouchou and Pichoir (1991). The crystals were analysed with a beam current of 15 nA using a focused beam and a counting time of 10 s on peak and background. For glass analyses, a special procedure was applied. In order to minimize the migration and volatilization of the alkali elements, the beam current was set to 6 nA. The counting time was 2 s for Na and K and 5 s for the other elements (Si, Ti, Al, Fe, Mn, Mg, Ca). Whenever possible, a defocused beam with a spot size of 10 μm was used. For small melt pools, a beam diameter of 1–5 μm was used, and Na-loss was calibrated with the help of correction factors obtained by analyzing glasses of identical composition and known water contents. In low-temperature run products, obtaining of correct microprobe analyses was difficult due to small crystal size. These analyses were carefully screened using compositional and stoichiometric criteria. Modal proportions of the experimental melts were estimated by evaluating backscattered electron (BSE) images in combination with EDX X-ray mapping using the imaging program of the software package "INCA" provided by Oxford.

Results

Attainment of equilibrium

The achievement of global equilibrium in melting experiments is problematic when using starting material that is too coarse-grained (see Johannes and Koepke 2001, and references therein). Coarse-grained starting material (e.g., ~50 μm) results in relatively large experimental crystals, well suited for electron microprobe analyses, but often with cores of unreacted starting material leading to an attainment of only local equilibrium. Very fine-grained starting material (e.g., ~1 μm) achieves global equilibrium conditions, but leads to the development of only very tiny crystals, making the microprobe work more difficult, and preventing reliable microprobe analyses of phases from near-solidus runs (Koepke et al. 2003). A series of experiments at 1,020 °C was performed using < 2, 2–10, and 10–50 μm starting material to study the effect of grain size of the starting material on the kinetics of the melting reaction (Table 2). All experimental results show the presence of the same phases, but with different grain sizes and subtly different compositions.

With increased grain size of the starting material, an increase in mineral zoning is observed. Olivine shows a diffuse zoning structure with Fe-rich inner parts and Mg-rich outer zones while clinopyroxene sometimes shows core/rim structures with a sharp boundary in between as a result of dissolution/precipitation processes (Fig. 1). The cores of the zoned minerals correspond to unreacted starting material while the rims show the same

Table 2 Summary of partial melting experiments

Run no.	T (°C)	XH_2O	fH_2[1)] (bar)	Run time (h)	Run products[b]	Melt fraction[c]
Starting material: gabbro 61a, 2–10 μm[d]						
1	900	1	n.a.	67	Plag, amph, opx, glass	< 10
2	940	1	9.7	68	Plag, amph, opx, glass	11
3	980	1	12.1	48	Ol, cpx, plag, amph, glass	43
4	1020	1	12.7	65	Ol, cpx, plag, glass	61
5	1060	1	5.8	24	Ol, glass	95
19	980	0.8	11.7	65	Ol, cpx, plag, amph, glass	< 10
20	980	0.6	11.7	65	Ol, cpx, plag, opx, amph, glass	< 10
21	980	0.4	11.7	65	Ol, cpx, plag, opx, amph, glass	< 10
Starting material: olivine gabbro 101, 2–10 μm[d]						
6	900	1	n.a.	67	Ol, plag, amph, opx, glass	< 10
7	940	1	9.7	68	Ol, plag, amph, glass	21
8	980	1	12.1	48	Ol, plag, glass	27
9	1,020	1	12.7	65	Ol, plag, glass	50
10	1,060	1	5.8	24	Ol, plag, glass	60
Starting material: gabbro 923A, 2–10 μm[d]						
11	900	1	n.a.	67	Plag, amph, opx, glass	< 10
12	940	1	9.7	68	Plag, amph, opx, glass	19
13	980	1	12.1	48	Ol, cpx, plag, glass	46
14	1,020	1	12.7	65	Ol, cpx, plag, glass	65
15	1,060	1	n.a.	24	Ol, cpx, plag, glass	60
Starting material: gabbro 923A, < 2 μm[d]						
16	1,020	1	12.0	24	Ol, cpx, plag, glass	–[e]
Starting material: gabbro 923A, 10–50 μm[d]						
17	1,020	1	12.0	24	Ol, cpx, plag, glass	–[e]

[a] fH_2 of the run, measured with the help of the H_2 membrane; *n.a.* not analyzed
[b] Abbreviations: *ol* Olivine, *plag* plagioclase, *cpx* clinopyroxene, *opx* orthopyroxene, *amph* amphibole
[c] Melt fraction in vol%, estimated from backscattered electron images
[d] Grain size fraction (separated with the help of the Atterberg sedimentation method)
[e] Melt fraction was not estimated

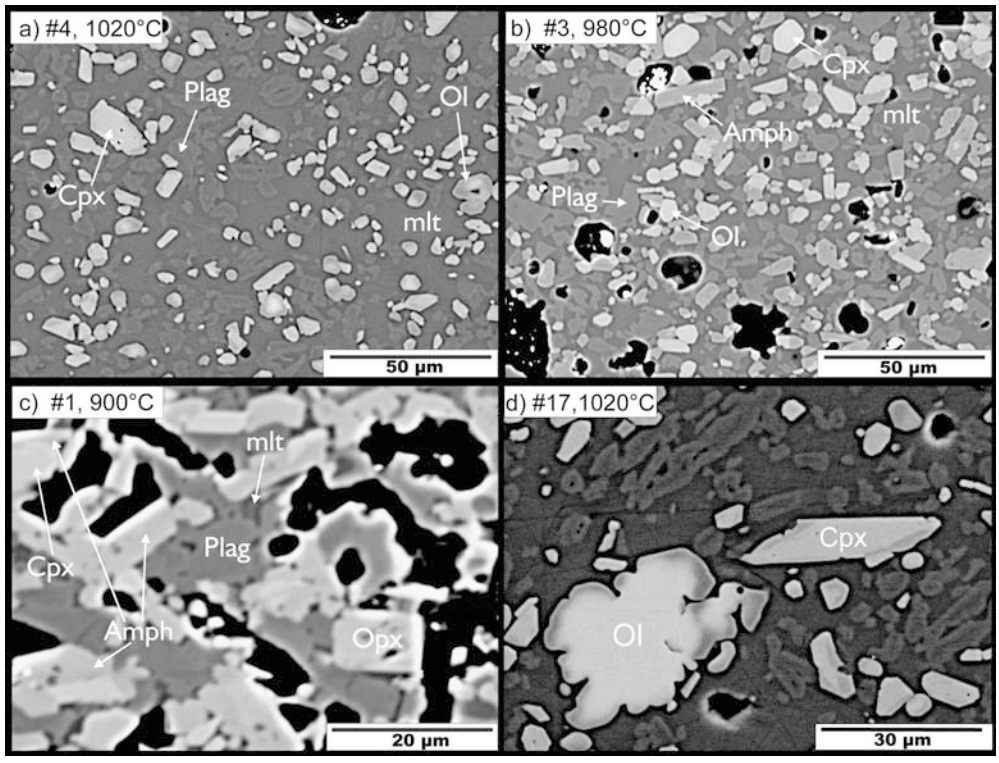

Fig. 1 Backscattered electron images of run products of partial melting experiments. **a–c** Sample 61a as starting material; grain size 2–10 µm. Cpx and plag in Fig. 2c are relics of the starting material; *cpx* is mantled by new amph, while plag shows very tiny rims of new An-rich plag, not seen in this image. **d** sample 923A as starting material; grain size 10–50 µm. Large grains of relics of ol and cpx from the starting material are observable. Ol shows diffusive zoning while cpx is affected by dissolution/precipitation processes. See text for details. *Ol* Olivine; *Cpx* clinopyroxene; *Opx* orthopyroxene; *Plag* plagioclase; *Amph* amphibole; *mlt* melt

composition as the newly formed idiomorphic crystals that represent the equilibrium composition. Plagioclase sometimes shows typical "sieve" structures (Johannes et al. 1994) with tiny melt pods within the larger grains. At 900 and 940°C in the runs with starting compositions 61a and 923A, only very thin zones of newly formed plagioclase around melt pods could be observed, which were too small for reliable electron microprobe analyses. Yet, EDX profiles through such zones show that the newly formed plagioclases are richer in An than the starting plagioclase. Our results confirm the well-known problematic behavior of plagioclase during partial melting experiments at lower temperatures that prevents the achievement of a global equilibrium (e.g., Johannes and Koepke 2001).

The best results were obtained with the charge 2–10 µm, which was used as starting material for the melting experiments. Bulk chemical analyses of the 2–10 µm charge show that the composition is the same as that of the bulk rock, indicating that no chemical fractionation occurred due to the separation process. However, the presence of unreacted minerals of the starting gabbros as cores within newly formed phases could not be avoided completely. In particular, at low temperatures, the identification of newly formed and relic phases was difficult (see Fig. 1). In these runs, we used compositional and textural criteria (e.g., reaction rims of orthopyroxene and amphibole around relic clinopyroxene) for distinguishing between stable and relict phases.

Several lines of evidence suggest that an approach to at least local equilibrium (due to the presence of relict phases) was attained in our experiments. (1) The newly formed crystal phases are homogeneous and euhedral. (2) Rims of newly formed phases around relic phases show the same composition as newly formed euhedral crystals (e.g., olivine in Fig. 1). (3) The glass shows constant compositions within the counting statistics of the microprobe analyses, irrespective of location within the sample. (4) All compositions of the newly formed phases vary systematically with temperature. (5) Iron loss could be avoided due to the relative high fO_2 and the use of capsules of Au ($< 1{,}060$ °C) and $Au_{80}Pd_{20}$ (1,060 °C) pre-saturated with iron (for details see Berndt et al. 2002). (6) Element partitioning data (e.g., between amphibole and melt or plagioclase and melt, see below) correspond to expected values from literature. (7) The formation of quench crystals was avoided, so that there was no need to distinguish between quench and stable phases or performing integrative measurements of glass and quench crystals, such as in previous studies of basaltic systems (e.g., Helz 1976).

Phase relations

A listing of the experimental conditions is given in Table 2 and the experimental results are given in Table 3. BSE images of the experimental products as a function of temperature of one starting gabbro (61a) are shown in Fig. 1. Melt coexisting with crystals was observed in all run products (Fig. 2).

It is obvious from Fig. 2 that the phase assemblages depend on the bulk composition. Whereas the olivine

Table 3 Composition of the experimental phases and of the minerals of the starting material

Run no.	Temp. [a]XH_2O	Phase	n[b]	SiO_2		TiO_2		Al_2O_3		FeO^{tot}		MnO	MgO		CaO		Na_2O		K_2O		P_2O_5		Total[c]	X[d]
Starting material: gabbro 61a																								
1[e]	900	Opx	3	53.29	(0.88)	0.21	(0.18)	1.72	(0.17)	18.92	(0.75)	0.46	(0.07)	23.52	(1.18)	1.98	(0.67)	0.06	(0.02)					100.15	68.9
		Amph	4	47.18	(0.90)	0.63	(0.08)	8.82	(0.88)	11.30	(0.20)	0.20	(0.05)	16.52	(0.65)	10.54	(0.33)	1.94	(0.16)	0.07	(0.01)			97.21	72.3
		Glass	3	67.38	(0.68)	0.14	(0.01)	17.02	(0.43)	4.09	(0.30)	0.09	(0.09)	1.87	(0.30)	5.61	(0.05)	3.42	(0.26)	0.22	(0.02)	0.16	(0.03)	100.00	48.9
2[e]	940	Opx	1	54.77		0.35		1.34		15.71		0.36		26.41		1.41								100.34	75.0
		Amph	4	45.72	(0.77)	0.67	(0.06)	10.75	(0.46)	10.16	(0.35)	0.20	(0.05)	16.56	(0.36)	10.97	(0.23)	2.40	(0.10)	0.04	(0.02)			97.46	74.4
		Glass	3	60.79	(2.08)	0.18	(0.04)	19.48	(0.39)	5.67	(0.13)	0.11	(0.06)	2.50	(0.40)	6.99	(0.30)	3.79	(0.13)	0.26	(0.01)	0.23	(0.08)	100.00	48.1
3	980	Ol	4	39.30	(0.32)			0.04	(0.04)	21.13	(0.69)	0.27	(0.05)	39.13	(0.35)	0.45	(0.32)							100.33	76.8
		Plag	5	48.72	(0.39)			32.63	(0.39)	0.45	(0.07)			0.10	(0.03)	16.24	(0.35)	2.45	(0.19)					100.59	78.5
		Cpx	4	52.08	(0.12)	0.18	(0.03)	2.55	(0.30)	5.90	(0.16)	0.16	(0.05)	16.18	(0.21)	21.87	(0.33)	0.26	(0.04)					99.18	83.0
		Amph	6	45.31	(0.54)	0.83	(0.09)	11.81	(0.42)	7.11	(0.37)	0.09	(0.03)	17.85	(0.32)	11.87	(0.29)	2.68	(0.07)	0.03	(0.01)			97.59	81.7
		Glass	9	57.61	(0.32)	0.34	(0.04)	19.34	(0.20)	6.05	(0.32)	0.13	(0.11)	3.76	(0.27)	8.06	(0.24)	4.59	(0.26)	0.12	(0.04)			100.00	56.6
4	1020	Ol	5	39.76	(0.36)			0.07	(0.05)	15.45	(0.27)	0.24	(0.05)	43.43	(0.82)	0.34	(0.11)							99.29	83.4
		Plag	4	47.06	(0.62)			33.43	(0.61)	0.43	(0.12)			0.21	(0.16)	16.71	(0.23)	2.04	(0.16)					99.89	81.8
		Cpx	7	52.84	(0.43)	0.26	(0.07)	2.92	(0.34)	4.27	(0.25)	0.14	(0.05)	16.53	(0.24)	22.80	(0.20)	0.24	(0.07)					100.01	87.3
		Glass	8	53.01	(0.39)	0.40	(0.04)	20.32	(0.38)	5.40	(0.38)	0.07	(0.07)	5.46	(0.19)	11.27	(0.27)	3.99	(0.16)	0.10	(0.04)			100.00	68.0
5	1060	Ol	4	41.23	(0.22)					11.33	(0.18)	0.20	(0.07)	45.83	(0.14)	0.29	(0.03)							98.88	87.8
		Glass	9	51.88	(0.39)	0.41	(0.05)	17.95	(0.17)	6.86	(0.50)	0.09	(0.06)	7.38	(0.13)	12.32	(0.22)	3.05	(0.30)	0.07	(0.04)			100.00	69.3
Natural		Ol	21	38.15	(0.14)					26.31	(0.33)	0.39	(0.05)	36.10	(0.25)	0.04	(0.01)							100.99	71.0
rock		Plag	25	54.45	(0.23)	0.07	(0.01)	28.63	(0.15)	0.29	(0.06)			0.03	(0.02)	11.53	(0.16)	5.23	(0.11)	0.06	(0.01)			100.29	54.7
		Cpx	17	51.89	(0.23)	0.83	(0.07)	2.68	(0.08)	7.73	(0.35)	0.22	(0.05)	15.09	(0.36)	21.61	(0.79)	0.45	(0.04)					100.50	77.7
Starting material: olivine gabbro 101																								
6	900	Ol	5	39.03	(0.29)			0.32	(0.30)	20.88	(0.20)	0.32	(0.02)	39.75	(0.46)	0.26	(0.14)							100.55	77.2
		Plag	2	48.63	(0.81)	0.03	(0.02)	32.89	(0.53)	0.44	(0.08)			0.06	(0.03)	15.74	(0.87)	2.55	(0.59)					100.34	77.2
		Opx	5	52.66	(0.33)	0.26	(0.10)	5.11	(0.75)	13.60	(0.36)	0.32	(0.01)	27.88	(0.17)	0.55	(0.07)							100.38	78.5
		Amph	4	44.13	(0.54)	0.14	(0.07)	13.57	(0.86)	10.74	(0.50)	0.17	(0.06)	14.41	(0.40)	11.69	(0.26)	2.21	(0.07)	0.13	(0.03)			97.19	70.5
		Glass	2	62.33	(0.60)	0.12	(0.03)	22.43	(0.63)	3.09	(0.03)	0.03	(0.10)	2.19	(0.28)	5.14	(0.47)	3.00	(0.07)	1.26	(0.26)	0.40	(0.09)	100.00	59.8
7	940	Ol	4	39.99	(0.29)			0.07	(0.03)	20.19	(0.26)	0.34	(0.06)	39.67	(0.42)	0.18	(0.04)							100.43	77.8
		Plag	3	48.53	(0.62)	0.03	(0.01)	32.98	(0.19)	0.48	(0.05)			0.03	(0.02)	16.50	(0.37)	2.33	(0.20)	0.03	(0.03)			100.90	79.6
		Amph	3	43.84	(0.85)	0.11	(0.02)	15.25	(0.90)	9.35	(0.55)	0.17	(0.04)	14.58	(0.25)	11.73	(0.28)	2.57	(0.10)	0.12	(0.01)			97.72	73.5
		Glass	8	60.30	(0.46)	0.56	(0.06)	20.87	(0.61)	3.89	(0.18)	0.08	(0.05)	3.44	(0.31)	5.48	(0.40)	3.71	(0.12)	1.61	(0.09)	0.07	(0.04)	100.00	65.0
8	980	Ol	5	39.46	(0.28)			0.06	(0.05)	18.73	(0.35)	0.28	(0.05)	41.37	(0.39)	0.20	(0.03)							100.11	79.7
		Plag	4	46.38	(0.39)			34.33	(0.45)	0.44	(0.14)			0.07	(0.03)	17.74	(0.36)	1.57	(0.15)	0.03	(0.02)			100.55	86.1
		Glass	6	57.18	(0.36)	0.49	(0.04)	21.16	(0.52)	4.79	(0.27)	0.12	(0.12)	3.94	(0.13)	6.95	(0.20)	4.39	(0.25)	0.98	(0.06)			100.00	63.3
9	1020	Ol	3	39.68	(0.15)			0.34	(0.45)	14.96	(0.52)	0.19	(0.01)	42.71	(1.14)	0.36	(0.22)							98.24	83.6
		Plag	4	45.32	(0.23)			34.68	(0.47)	0.65	(0.22)			0.13	(0.13)	17.73	(0.40)	1.34	(0.10)	0.04	(0.01)			99.90	87.7
		Glass	7	52.60	(0.23)	0.31	(0.02)	22.27	(0.21)	6.40	(0.46)	0.07	(0.08)	5.46	(0.20)	8.46	(0.23)	3.77	(0.14)	0.65	(0.08)			100.00	64.2
10	1060	Ol	4	40.72	(0.05)			0.04	(0.01)	14.49	(0.26)	0.21	(0.04)	43.37	(0.34)	0.20	(0.02)							99.03	84.2
		Plag	8	46.89	(0.53)			34.04	(0.39)	0.62	(0.09)			0.13	(0.02)	17.74	(0.43)	1.53	(0.21)	0.03	(0.01)			100.97	86.3
		Glass	7	51.22	(1.30)	0.29	(0.05)	20.98	(0.26)	8.44	(0.41)	0.18	(0.11)	6.05	(0.40)	9.09	(0.47)	3.24	(0.15)	0.52	(0.07)			100.00	60.1
Natural		Ol	14	38.59	(0.43)					21.30	(0.53)	0.33	(0.06)	39.71	(0.32)	0.06	(0.02)							99.99	76.9
rock		Plag	20	50.25	(1.19)	0.06	(0.02)	31.57	(0.82)	0.11	(0.05)					14.46	(1.01)	3.49	(0.59)	0.05	(0.03)			99.99	69.4
		Cpx	14	51.03	(0.32)	1.29	(0.08)	3.31	(0.17)	5.67	(0.42)	0.18	(0.04)	16.23	(0.52)	21.49	(1.02)	0.35	(0.06)					99.55	83.6
Starting material: gabbro 923A																								
11[e]	900	Opx	4	53.57	(0.46)	0.25	(0.13)	1.27	(0.38)	18.47	(0.51)	0.38	(0.05)	25.27	(0.54)	1.29	(0.40)							100.50	70.9
		Amph	4	45.39	(0.98)	0.59	(0.14)	10.93	(0.31)	11.55	(0.62)	0.16	(0.02)	15.61	(0.39)	10.87	(0.14)	2.24	(0.09)	0.20	(0.02)			97.54	70.7
		Glass	2	66.40	(0.06)	0.10	(0.06)	18.03	(0.59)	4.27	(0.44)	0.12	(0.07)	2.30	(0.37)	5.28	(0.12)	2.73	(0.12)	0.60	(0.12)	0.17	(0.12)	100.00	53.0
12[e]	940	Opx	3	55.10	(0.53)	0.22	(0.08)	1.95	(0.79)	16.30	(1.39)	0.31	(0.03)	25.58	(0.87)	1.33	(0.09)							100.79	73.7

Table 3 (Contd.)

Run no.	Temp. [a]XH_2O	Phase	n[b]	SiO_2		TiO_2		Al_2O_3		FeO^{tot}		MnO	MgO		CaO		Na_2O		K_2O		P_2O_5				Total[c]	X[d]
		Amph	2	45.65	(0.17)	0.37	(0.12)	9.44	(0.01)	13.71	(0.02)	0.27	(0.01)	14.06	(0.01)	11.43	(0.42)	2.03	(0.14)	0.19	(0.04)			97.14	64.6
		Glass	7	60.88	(0.57)	0.35	(0.01)	19.64	(0.74)	4.99	(0.47)	0.15	(0.09)	2.62	(0.28)	6.54	(0.34)	4.40	(0.32)	0.33	(0.05)	0.10	(0.04)	100.00	52.4
13	980	Ol	5	38.88	(0.26)			0.04	(0.04)	22.82	(0.31)	0.25	(0.04)	38.14	(0.19)	0.22	(0.03)							100.35	74.9
		Plag	5	48.47	(0.37)	0.04	(0.02)	32.54	(0.29)	0.73	(0.09)	0.00	(0.06)	0.16	(0.11)	16.11	(0.26)	2.38	(0.09)					100.43	78.8
		Cpx	4	52.62	(0.66)	0.25	(0.04)	2.27	(0.36)	6.43	(0.09)	0.13	(0.06)	16.10	(0.31)	21.87	(0.25)	0.21	(0.05)					99.89	81.7
		Glass	8	58.01	(0.64)	0.48	(0.03)	19.16	(0.33)	6.19	(0.31)	0.11	(0.08)	3.66	(0.42)	7.47	(0.25)	4.77	(0.23)	0.17	(0.03)			100.00	55.3
14	1020	Ol	5	39.62	(0.18)			0.15	(0.14)	17.20	(0.83)	0.20	(0.07)	41.40	(0.44)	0.38	(0.10)							98.95	81.1
		Plag	4	47.19	(0.22)			33.49	(0.25)	0.55	(0.05)			0.15	(0.14)	16.85	(0.20)	1.96	(0.14)					100.19	82.6
		Cpx	3	52.53	(0.46)	0.28	(0.07)	2.77	(0.32)	5.66	(0.65)	0.14	(0.02)	15.83	(0.28)	22.40	(0.26)	0.22	(0.01)					99.81	83.3
		Glass	10	54.14	(0.50)	0.33	(0.05)	19.62	(0.26)	6.80	(0.28)	0.05	(0.10)	4.85	(0.12)	10.19	(0.33)	3.89	(0.25)	0.13	(0.03)			100.00	60.0
15	1060	Ol	4	39.87	(0.28)					14.43	(0.95)	0.22	(0.02)	45.38	(0.67)	0.34	(0.03)							100.24	84.9
		Plag	7	45.83	(0.41)			33.62	(0.54)	0.51	(0.09)			0.21	(0.13)	17.39	(0.18)	1.65	(0.10)					99.19	85.3
		Cpx	7	52.08	(0.35)	0.19	(0.03)	3.01	(0.35)	4.16	(0.40)	0.08	(0.04)	16.86	(0.24)	22.84	(0.42)	0.21	(0.02)					99.43	87.8
		Glass	8	52.55	(0.39)	0.32	(0.02)	19.76	(0.16)	6.17	(0.18)	0.09	(0.07)	6.03	(0.18)	11.09	(0.25)	3.95	(0.21)	0.04	(0.01)			100.00	67.2
Natural rock		Ol	3	37.66	(0.15)					29.89	(0.76)	0.46	(0.01)	32.87	(0.91)	0.07	(0.03)							100.95	66.2
		Plag	3	55.40	(0.14)	0.05	(0.01)	28.68	(0.24)	0.26	(0.04)					11.19	(0.22)	5.46	(0.13)	0.05	(0.01)			101.09	53.0
		Cpx	3	51.59	(0.29)	0.83	(0.13)	2.41	(0.20)	8.91	(0.42)	0.29	(0.08)	14.63	(0.27)	21.25	(0.59)	0.42	(0.03)					100.33	74.5
		Amph	3	42.87	(0.26)	4.18	(0.13)	11.34	(0.25)	12.42	(0.28)	0.15	(0.04)	13.11	(0.04)	11.63	(0.14)	2.68	(0.10)	0.16	(0.03)			98.54	65.3
Runs with reduced XH_2O (sample 61a, only 980 °C)																									
19[f]	0.8	Ol	3	38.09	(0.22)			0.06	(0.03)	23.89	(0.30)	0.37	(0.04)	36.08	(0.19)	0.28	(0.05)							98.77	72.9
		Plag	1	51.01		0.03		29.86		0.90				0.31		13.41		3.59		0.03				99.14	67.2
		Cpx	4	50.85	(0.11)	0.85	(0.09)	2.86	(0.23)	7.10	(0.27)	0.22	(0.04)	14.56	(0.18)	21.82	(0.29)	0.43	(0.05)					98.69	78.5
		Amph	5	46.17	(0.91)	0.89	(0.14)	10.17	(0.79)	9.09	(1.43)	0.09	(0.02)	17.24	(0.54)	10.73	(1.04)	2.50	(0.27)	0.11	(0.07)			96.99	77.2
20[f]	0.6	Ol	3	38.15	(0.56)			0.31	(0.41)	25.92	(0.18)	0.37	(0.03)	34.47	(0.31)	0.28	(0.07)							99.50	70.3
		Plag	3	52.59	(1.54)	0.07	(0.03)	29.18	(0.94)	1.12	(0.56)			0.37	(0.29)	12.43	(1.00)	4.00	(0.91)	0.05	(0.01)			99.81	63.0
		Cpx	3	50.96	(0.09)	1.08	(0.11)	2.98	(0.08)	7.44	(0.12)	0.24	(0.04)	14.33	(0.22)	21.86	(0.37)	0.49	(0.04)					99.38	77.4
		Opx	3	53.90	(0.45)	0.29	(0.15)	1.28	(0.11)	16.48	(0.81)	0.37	(0.05)	25.67	(0.42)	1.09	(0.42)	0.02	(0.01)					99.10	73.5
		Amph	4	47.38	(0.72)	0.85	(0.09)	9.55	(1.15)	9.37	(0.72)	0.15	(0.03)	17.60	(1.06)	9.74	(0.66)	2.42	(0.09)	0.08	(0.03)			97.14	77.0
21[f]	0.4	Ol	4	37.88	(0.24)			0.22	(0.28)	27.28	(0.72)	0.38	(0.04)	33.75	(0.69)	0.27	(0.07)							99.78	68.8
		Plag	1	51.96		0.05		29.03		0.81				0.08		12.84		3.90		0.06				98.73	64.3
		Cpx	5	51.27	(0.21)	0.91	(0.12)	3.07	(0.21)	7.79	(0.60)	0.19	(0.07)	14.72	(0.33)	21.00	(0.70)	0.45	(0.11)					99.40	77.1
		Opx	3	53.44	(0.06)	0.29	(0.03)	1.50	(0.22)	17.75	(0.38)	0.36	(0.03)	24.98	(0.18)	0.98	(0.09)							99.30	71.5
		Amph	4	46.39	(1.59)	1.17	(0.37)	9.76	(1.60)	10.34	(0.92)	0.14	(0.08)	16.67	(0.49)	10.44	(1.27)	2.43	(0.29)	0.12	(0.04)			97.46	74.2

Missing values indicate measurements below the detection limit of the microprobe
Abbreviations:*ol* olivine; *plag* plagioclase;*cpx* clinopyroxene; *opx* orthopyroxene; *amph* amphibole
[a]XH_2O only in the experimental series with $XH_2O < 1$ performed at 980 °C
[b]Number of analyses; numbers in parentheses are standard deviations
[c]Glass analyses were normalized to anhydrous totals of 100 wt% to facilitate comparisons
[d]Compositional parameter in mol%: olivine—forsterite content; plagioclase—anorthite content; pyroxene and amphibole—Mg#; glass—100×MgO/(MgO + FeO) with FeO = 0.85 Fe2O3 (molar)
[e]These runs contain newly formed tiny plagioclase; due to the small crystal size reliable microprobe analyses were not possible
[f]The melt pools in these runs are too tiny for reliable microprobe analyses

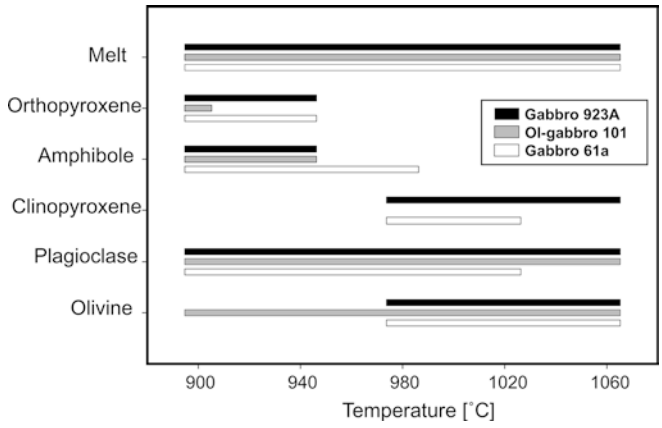

Fig. 2 Stabilities of the experimental phases in the products of partial melting experiments

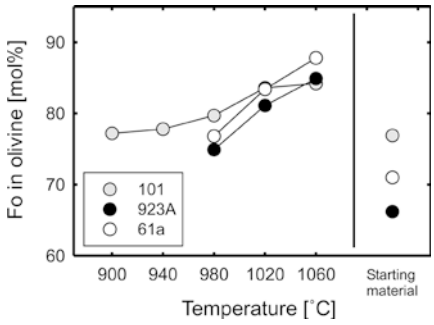

Fig. 3 Forsterite content in olivines of the experimental products and of the natural starting material. *Error bars* are smaller than the symbols

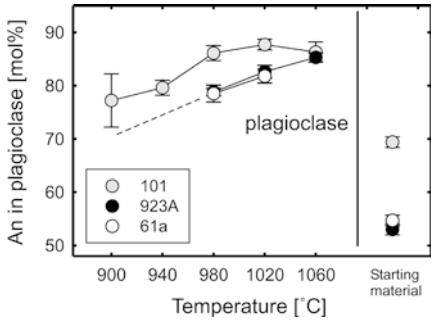

Fig. 4 Anorthite content in plagioclases of the experimental products and of the natural starting material. The *dashed line* is the extrapolation of the expected compositions in the samples 61a and 923A to lower temperatures, since in the runs at 940 and 900 °C the newly formed plagioclases were too small for microprobe analyses

gabbro 101, which is characterized by a more refractory chemical composition, has clinopyroxene in the natural rock, no clinopyroxene is observed in the experimental products. Thus, by only adding water to this system, the crystallization of clinopyroxene is suppressed, leading to the formation of typical troctolites, provided that crystals and melt are separated from each other. The run products of the two other compositions (61a and 923A) show at higher temperatures (≥980 °C and ≥940 °C, respectively) a crystal assemblage consisting of olivine, plagioclase, and clinopyroxene, resulting in typical olivine–clinopyroxene gabbros after removing the melt.

Both amphibole and orthopyroxene are stable at lower temperatures in all investigated compositions. In the more evolved systems 61a and 923A, the appearance of orthopyroxene is accompanied by the disappearance of olivine, while in the more refractory system, 101 olivine is stable down to the lowest temperature. It should be noted that at water-saturated conditions in all of the investigated systems clinopyroxene and orthopyroxene stabilities did not overlap. As a consequence, if the melt is removed from such wet magmas at lower temperature, the generated restite rocks are norites. This is not the case at reduced water-activities (runs 20, 21), where at 980 °C clinopyroxene coexists with orthopyroxene.

Phase chemistry

Olivine

Figure 3 shows the dependence of the olivine composition on the run temperature. The Fo contents are generally higher than in the natural samples increasing with temperature. This is attributed to the influence of water in our experiments, which enhances the Fo contents in olivine for a given temperature (for details see Berndt 2002), in comparison to the assumed "dry" crystallization of the natural gabbros. In addition, the oxidizing conditions in our experiments compared to the reducing conditions during the forming of the gabbros also result in the formation of olivines richer in Fo content. Newly formed olivines always show elevated CaO contents (0.2–0.5 wt%), in contrast to the natural olivines of the starting material (0.04–0.07 wt%). At the lowest investigated temperatures (900 and 940 °C), olivine is only stable in the most refractory sample 101. In this sample, the overall increase in Fo content with temperature (from 900 to 1,060 °C) is relatively small comprising only 7 mol%, which is expressed by a relatively flat line in Fig. 3. In contrast, the temperature-induced increase (from 980 to 1,060 °C) in Fo content in the more evolved composition (sample 61a and 923A) results in steeper curves (Fig. 3).

Plagioclase

As in the case of olivine, the experimental plagioclases are generally more An-rich compared to the natural plagioclases, which are assumed to be crystallized at relatively "dry" conditions in typical oceanic gabbros (Fig. 4). This is due to the well-known effect of water, which increases the An contents in plagioclase (e.g., Turner and Verhoogen 1960; Carmichael et al. 1974; Panjasawatwong et al. 1995; Martel et al. 1998; Scaillet

and Evans 1999; Berndt et al. 2001; Berndt 2002). For example, the An contents of our experimental plagioclases lie systematically about 10 to 30 mol% above the calculated An values for dry systems according to Panjasawatwong et al. (1995) as a result of water-saturated condition in our experiments. According to Sisson and Grove (1993), direct influence of H_2O on plagioclase-liquid equilibrium compositions is expressed by elevated $Kd^{Pl-Melt}_{Ca-Na}$ values [defined as molar $(Ca/Na)_{plag}/(Ca/Na)_{melt}$] in comparison to dry systems. The compositions of our experimental plagioclase-melt pairs lead to an average $Kd^{Pl-Melt}_{Ca-Na}$ value of 4.4 which is in agreement with Sisson and Grove (1993), who obtained a Kd value of 3.4 for plagioclase-melt pairs in high-alumina basaltic systems with melts containing ~4 wt% water. Newly formed plagioclases always show distinctly higher FeO contents than the starting plagioclase.

Pyroxene

Newly formed clinopyroxene is present in runs performed with the more evolved gabbros 61a and 923A at temperatures ≥980 °C. At lower temperatures, clinopyroxene becomes unstable, as indicated by reaction rims of amphibole and orthopyroxene around relic clinopyroxenes from the starting material. This is in contrast to a hydrous MORB system, where the paragenesis clinopyroxene–amphibole is stable down to the solidus at water-saturated conditions (Berndt 2002). As observed for olivine and plagioclase, the experimental clinopyroxene shows a more refractory composition compared to the natural one with an Mg# similar to that of the corresponding olivine in the same run (Table 3).

Orthopyroxene appears in all runs at low temperatures. In the more evolved systems 61a and 923A, the appearance of orthopyroxene is accompanied by the disappearance of olivine. This the well-known reaction relationship between olivine and orthopyroxene as temperature decreases in basaltic systems (e.g., Toplis and Carroll 1995; Berndt 2002). Only in one run at 900 °C performed with the olivine gabbro 101 as starting material do orthopyroxene and olivine coexist, although the modal amount of olivine in this run is markedly decreased. The Mg# of olivine and orthopyroxene in this run are nearly identical (77.2 and 78.5, respectively).

Amphibole

Experimental amphiboles with pargasitic to edenitic compositions are stable in all three systems at temperatures ≤ 980 °C (according to the classification of Leake et al. 1997). In the systems 61a and 101, tetrahedral Al and Na on the A-site of the amphiboles increase with temperature, in agreement with previous experimental studies (e.g., Blundy and Holland 1990; Sisson and Grove 1993; Ernst and Liou 1998). The maximum TiO_2 content in the amphiboles of all three gabbroic systems is relatively low (< 0.8 wt%), which is due to the low TiO_2 content of the corresponding melts (< 0.6 wt%). These contents are significantly lower than the TiO_2 concentration of 4.2 wt% in the pargasites occurring in the natural gabbro 923 (Table 3). Sisson and Grove (1993) emphasized that Al/Si in amphibole is linearly related to the Al/Si (molar) of the melt and can be described as $Kd^{Am-Melt}_{Al-Si} = (AI/Si)_{amph}/(Al/Si)_{melt}$.. A calculated value of 0.81 ± 0.1 from seven coexisting liquid–amphibole pairs in our experiments is slightly lower than the Kd value of 0.94 ± 0.1 obtained by Sisson and Grove (1993) for liquid-amphibole couples in compositions ranging from high-alumina basalt to high-silica rhyolite.

Melt

Under our experimental conditions, the water contents of the melts under water-saturation is 5–7 wt%, as estimated by the "difference-to-100%" method with the electron microprobe. With decreasing temperature the melt fraction decreases down to less than 10 vol% at the lowest investigated temperature. At the same time, the SiO_2 content of the melt continuously increases (Fig. 5) attaining at temperatures of 940 and 900 °C the concentration typical of oceanic plagiogranites according to the definition of Coleman and Donato (1979) in all three systems (Fig. 6). At 940 °C, the normalized melt SiO_2 contents of all systems range between 60.3 and 61.6 wt%, and at 900 between 63 and 68 wt%. Due to the small size of the melt pools, however, these analyses scatter considerably and are often influenced by neighboring crystals. Therefore, the averages of the runs in Table 3 show a poorer accuracy compared to those derived from runs performed at the higher temperature. K_2O also increases with decreasing temperature reaching concentrations of typical oceanic plagiogranites (0.2–0.6 wt%) in two samples (61a and 923A). In sample 101 the K_2O contents in the melt are significantly enhanced exceeding 1.5 wt% at 940 °C, which is much higher than typical of oceanic plagiogranites (Fig. 6). This is due to an elevated K_2O content in the source rock (0.31 wt%), which is relatively high compared with other typical

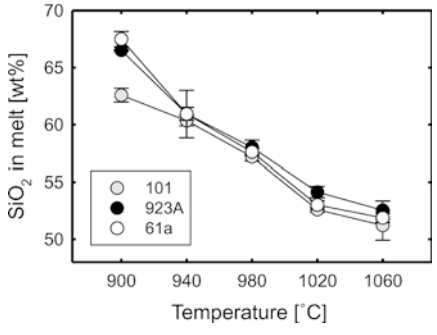

Fig. 5 SiO_2 content in the residual melts as a function of temperature (normalized to a total of 100 wt%)

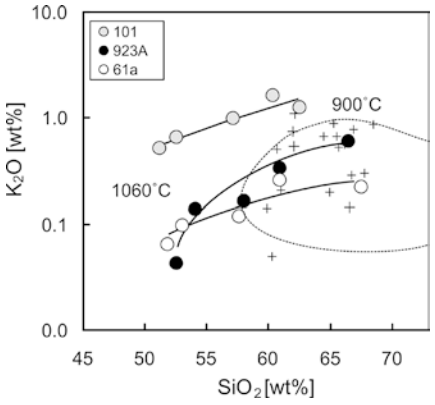

Fig. 6 Liquid lines of descent in the diagram K_2O versus SiO_2 (normalized to a total of 100 wt%). For each system, the left side of the trends correspond to the residual melts of the runs of 1,060 °C. The *crosses* represent natural plagiogranites from different tectonic settings listed in the Appendix. Included is the field for oceanic plagiogranites according to Coleman and Donato (1979)

oceanic gabbros from the Leg 176 (Ozawa et al. 1991; Dick et al. 2000; Natland and Dick 2002; Niu et al. 2002). The high amount of potassium in this sample is probably the result of contamination, because this rock shows distinct signs of alteration (see above, description of the starting material).

In a TAS diagram (Le Maitre 1989) the experimental melts of each sample clearly plot into the field of subalkaline rocks. Typically, their evolution trends show a slight decrease of total alkalis with increasing SiO_2. Probably, the reason for this is the hindrance in achieving global equilibrium in the low-temperature runs due to the presence of unreacted relict minerals. In an AFM diagram (Irvine and Baragar 1971) and in an FeO/(FeO + MgO) diagram (Miyashiro 1974) the experimental melts do not show any iron enrichment trend, leading to evolution trends comparable with those of typical calc-alkaline suites.

Discussion

Comparison with natural oceanic plagiogranites of different tectonic settings

For a comparison with natural oceanic plagiogranites we have compiled a database of plagiogranitic compositions from different tectonic settings. Beside plutonic plagiogranites from supra-subduction zone ophiolites and from the layer three of the recent oceanic crust drilled during an ODP cruise (Leg 176), the data set also contains plagiogranitic compositions of volcanic and subvolcanic rocks from spreading centers in mid-ocean ridge and back-arc basin environments. All these SiO_2-rich rocks are believed to be generated by fractional crystal differentiation from a primitive tholeiitic MORB-like source. In addition, plagiogranites generated by anatexis of mafic rocks are included, as well as analyses of experimental melts with plagiogranitic composition generated by partial melting of a primitive MORB (Dixon-Spulber and Rutherford 1983) or by crystallization experiments using a primitive MORB glass (Berndt 2002). For an appropriate comparison with our experimental melts, which range in SiO_2 between 60 and 67 wt%, our data compilation only includes silicic compositions with SiO_2 content below 70 wt%, since high-silicic plagiogranites are compositionally too diverse for a reliable comparison (e.g., the data set of Floyd et al. 1998, presenting analyses with SiO_2 contents up to 82 wt% often with MgO contents of < 0.1 wt%). Averages and selected analyses out of the data set are presented in the Appendix (Table 4). The whole database including the individual analyses is available from the authors upon request.

The experimental melts of runs below 940 °C generally show typical characteristics of oceanic plagiogranites with low K_2O concentrations (Fig. 6) except for sample 101 which show elevated K_2O contents. The high amount of potassium in this sample is probably the result of contamination, because this rock shows distinct signs of alteration (see above, description of the starting material). The experiments performed with this sample show the strongly incompatible behavior of potassium during melting. It is thus excluded that partial melting of hydrothermally altered gabbros or metagabbros is a reliable process for generating typical oceanic plagiogranites.

Remarkably, at 940 and 900 °C, the experimental melts are rather similar in composition (Table 3), in spite of the compositional differences of the starting materials, enabling the calculation of average melt compositions for the temperatures 900 and 940 °C (see Appendix, Table 4). For the comparison with natural plagiogranites of different tectonic settings, Harker diagrams were used. The experimental melts of this study generally overlap those of natural plagiogranites in terms of most major and minor elements (FeO^{tot}, MgO, CaO, Na_2O, K_2O, P_2O_5; see Fig. 7 for selected elements). Exceptions are Al_2O_3, which is high in the experimental melts, and both TiO_2 and FeO, which are markedly low in our experimental melts (Fig. 7). Interestingly, the same trend is indicated by plagiogranites of inferred anatectic origin (at least one sample in terms of Al_2O_3). This is a result of the refractory compositions of the gabbroic source rock, which is high in Al_2O_3 and low in TiO_2 and FeO. In particular, the low TiO_2 content is a general feature of typical oceanic gabbros of cumulate origin (e.g., 0.3–0.4 wt% TiO_2 in olivine gabbros from the Leg 176; Dick et al. 2000; except for ferrogabbros, see below). This clearly indicates that plagiogranitic suites generated by partial melting of "normal" oceanic gabbros should show, in addition to the lack of any iron enrichment (see above), low TiO_2 contents. This contrasts with the generally high TiO_2 contents of plagiogranitic volcanics and sub-volcanics (the "MOR" and "BAB" data points in Fig. 7). These are assumed to be products of crystal differentiation in a MORB system (e.g., Fornari et al. 1983). It also contrasts with the high TiO_2 concentration (> 1 wt%) of the

plagiogranitic experimental melts generated at ~950 °C, either by partial melting of MORB (Dixon-Spulber and Rutherford 1983) or by crystallization in a MORB system (Berndt 2002) under reducing condition. Thus, our experiments imply that TiO_2 is a key parameter for the discrimination between both processes: TiO_2 is low in anatectic plagiogranitic melts and high in those plagiogranites generated by differentiation of MORB.

Comparison with leucocratic rocks from the ODP hole 735B

Two of the gabbros used as starting material were samples of the hole 735B of the Leg 176 at SWIR (Dick et al. 2000). The ~1,500-m-long drilled section contains typically olivine gabbros, olivine pyroxene gabbros, and oxide gabbros as well as numerous small (a few millimeters to several centimeters thick) felsic veins, mostly of plagiogranitic composition with SiO_2 contents > 60 wt%. According to Niu et al. (2002), these veins represent SiO_2-enriched melts as late products of differentiation of MORB magmas (melt fraction = 10–15%). In Fig. 8, we compare these compositions with our averages for experimental melts obtained at 900 and 940 °C. The compositions of the Leg 176 plagiogranites are generally low in TiO_2 (and also in FeO^{tot}), as in our experimental melts. In contrast, compositions of experimental melts in a MORB system obtained at ~950 °C from Dixon-Spulber and Rutherford (1983) and Berndt (2002) also included in Fig. 8, are markedly higher in TiO_2 compared to the vast majority of the Leg 176 plagiogranites. Thus, Fig. 8 implies that the felsic veins at SWIR can be better explained by partial melting of gabbros than by late-stage differentiation. In particular, those samples which are relatively poor in SiO_2 (around 60 wt%) showing TiO_2 concentrations below 0.5 wt% can hardly be traced back to an origin by differentiation of a MORB basalt. One argument in favor of the late-stage differentiation model is that typical plagiogranitic veins occasionally bear apatite (and also zircons), which are assumed to represent typical products of late-stage crystallization. However, the plagiogranitic compositions from the SWIR are markedly poor in P_2O_5. They have contents very similar to the average of our experimental melts for 940 °C, distinctly lower than those P_2O_5 concentration for experimental melts in a MORB system obtained at ~950 °C (Fig. 8). This also points to an origin for the Leg 176 plagiogranites by partial melting of gabbro.

Further arguments for the partial melting model are based on the presence and composition of minerals left behind as traces of a potential partial melting process in so-called "high-temperature microscopic veins" (Maeda et al. 2002) or "igneous veins" (Robinson et al. 2002). Such veins are widely distributed throughout the drilled section with estimated temperatures based on pyroxene thermometry up to 1,000 °C (Maeda et al. 2002). Orthopyroxene and amphibole compositions of such

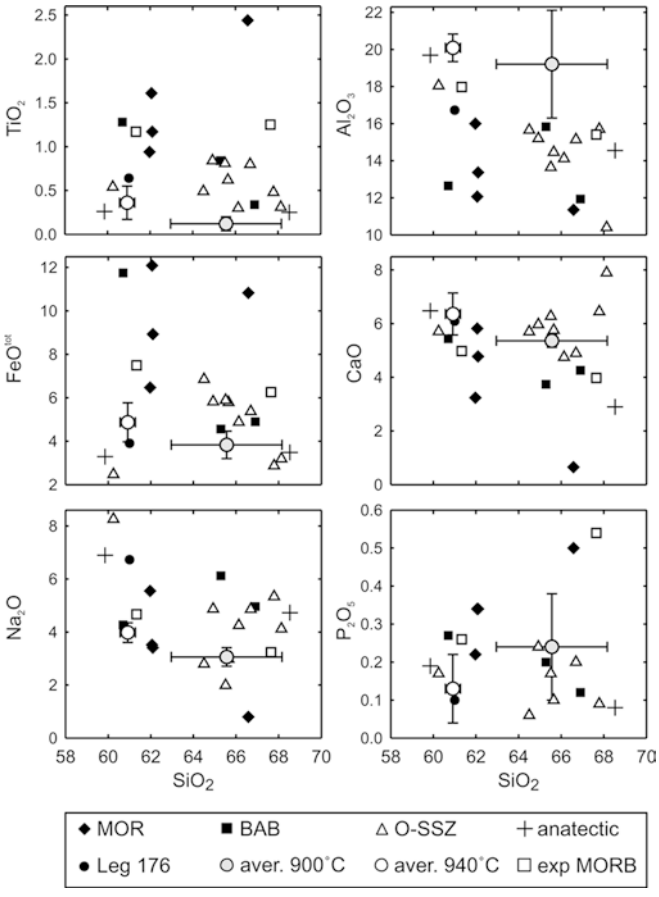

Fig. 7 Harker diagrams for selected element oxides (wt%). Average experimental melt composition of our runs at 900 and 940 °C [aver. 900 °C, aver. 940 °C]; experimental melts obtained at ~950 °C in a MORB system according to Berndt (2002) and Dixon-Spulber and Rutherford (1983) [exp MORB]; natural plagiogranites of different tectonic settings: mid-ocean ridge volcanic rocks [MOR]; back-arc basin volcanic rocks [BAB]; plutonites from supra-subduction zone ophiolites [O-SSZ]; anatectic plagiogranites from ophiolites [anatectic:]; average of the plagiogranites/felsic veins from Leg 176 at SWIR of Niu et al. (2002) [Leg 176]. Each data point of the natural plagiogranites represents a different location (average or representative sample). For details and references of the used data see Appendix

veins fit well with those of our experimental crystals coexisting with plagiogranitic melt at 900 to 980 °C. Figure 9 shows $(Na + K)_{A\text{-site}}$ against tetrahedral Al of selected amphiboles with edenitic/pargasitic compositions from both high-temperature veins and from our partial melting experiments. Also shown are 735B amphiboles of inferred magmatic origin (Maeda et al. 2002). Figure 9 shows the general compositional overlap of all these amphiboles. According to Maeda et al. (2002), beside pargasitic amphiboles, typical minerals in such high-temperature veins are orthopyroxene, clinopyroxene, and also An-rich plagioclase. Such minerals are also observed in our partial melting experiments, with similar compositions. Thus, the observed parageneses in high-temperature veins and the composition of their minerals are consistent with being a typical mineral paragenesis of a partial melting processes.

By carefully checking high-temperature veins of gabbros from Leg 176 with backscattered electron imaging, we actually found microstructures, which seem to indicate hydrous partial melting, as shown in Fig. 10 (sample R6a, ODP description: 176–735B-178R-6:132–138). The plagioclase in contact with the vein shows an irregular zone a few tens of microns thick that is significantly enriched in An (An_{76}), while clinopyroxene along the vein has reacted to orthopyroxene (Mg# = 75) and pargasite (Na + K on A = 0.73; Mg# = 74). The An-rich plagioclase, orthopyroxene, and pargasite are regarded as a typical crystal assemblage formed by a partial melting reaction. Striking is the compositional agreement with corresponding phases of those melting experiments using the gabbro 61a as starting material. Gabbro 61a shows a composition (olivine—Fo_{71}, plagioclase—An_{55}, clinopyroxene—Mg# = 78, Table 3) that matches well that of the sample R6a (olivine—Fo_{71}, plagioclase—An_{55}, clinopyroxene—Mg# = 80).

Run #2 performed at 940 °C has orthopyroxene (Mg# = 75), pargasite (Na + K on A = 0.68; Mg# = 74), and plagioclase (~An_{74}, extrapolated from Fig. 4, since the plagioclase of the 940 °C run was too small for microprobe analysis). Clinopyroxene was not stable in that run. The excellent fit between natural and experimental minerals implies melting temperatures of ~940 °C under water-saturated conditions. The melt, once formed, was probably removed due to pervasive mass transfer in such veins, which also acted as pathways for later hydrothermal fluids at various temperature (indicated by the presence of patches of chlorite within these veins, Fig. 10). Micron-sized "pools" of hornblende within the reaction zone between clinopyroxene and pargasite are interpreted as remnants of former melt pockets.

Genesis of plagiogranites by partial melting of gabbros: a major process in the oceanic crust?

Our experimental investigation shows that partial melting of typical oceanic gabbros can result in the formation of plagiogranitic melts, provided that (1) temperatures exceed ~900 °C and (2) that a water-rich fluid phase is present. Since point (1) is facilitated in high-temperature shear zones occurring in many locations in the environment of oceanic spreading centers (references see above), the question is whether enough water for triggering the melting process is available. To study the influence of water on the melting process, some runs with reduced aH_2O were also performed (at 980 °C; sample 61a; Tables 2, 3).

With reduced aH_2O the amount of melt decreases drastically, resulting in melt pools that are too small for reliable electron microprobe analysis. At a XH_2O of 0.4 in the fluid phase, the amount of melt is reduced to a few percent, being detectable only by performing careful EDX profiles through zones containing supposed melt. The effect of water on the melting reaction is thus significant: The run at 900 °C under water-saturated condition shows a larger melt volume than the corresponding

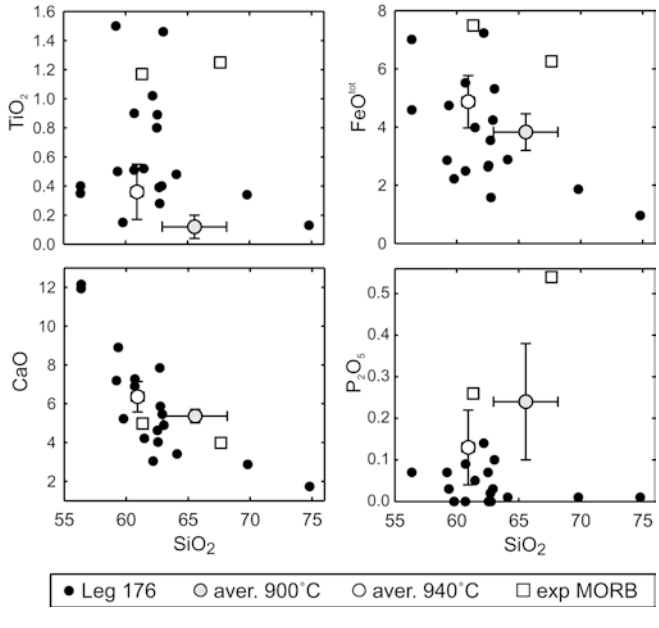

Fig. 8 Harker diagrams for selected element oxides (wt%). Average experimental melt compositions of our runs at 900 and 940 °C [aver. 900 °C, aver. 940 °C], for experimental melts obtained at ~950 °C in a MORB system according to Berndt (2002) and Dixon-Spulber and Rutherford (1983) [exp MORB], and for individual felsic veins with plagiogranitic composition from Leg 176 at SWIR of Niu et al. (2002) [Leg 176]

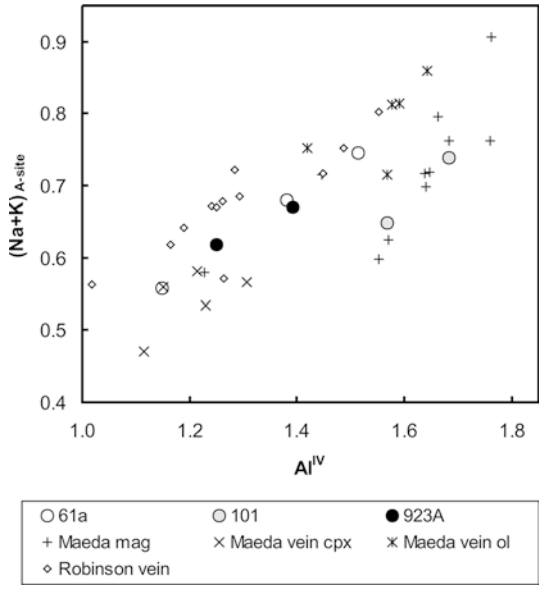

Fig. 9 Na + $K_{(A\text{-site})}$ versus tetrahedral Al for amphiboles of our partial melting runs for three (starting gabbro 61a) and two (starting gabbros 923A and 101) different temperatures and for amphiboles occurring in high-temperature veins within gabbros from the Leg 176 at SWIR. Data are from Maeda et al. (2002): magmatic amphiboles [mag], amphiboles from veins within clinopyroxene [vein cpx] and olivine [vein ol], and from Robinson et al. (2002): selected amphiboles with edenitic/pargasitic composition [vein]

run at 980 °C with a XH_2O of 0.4. Thus, larger volumes of plagiogranitic melts generated by partial melting of gabbros would only develop under high aH_2O.

It is possible to estimate how much bulk water is necessary to produce small volumes of water-rich melts as in our low-temperature experiments: At 200 MPa, a maximum of ~5 wt% water is soluble in a basaltic MORB-type melt (Berndt et al. 2002). Thus, for achieving a water-saturated melt with a fraction of ~10% (corresponding to a melting temperature of ~900 °C according to our experiments) a bulk water content of only 0.5 wt% is necessary. The same calculation for 100 MPa (corresponding to a depth of ~3 km), where the water solubility in a MORB melt is ~3 wt% (Berndt et al. 2002), leads to an even smaller bulk water content of only 0.3 wt%.

A possible source of water are high-temperature hydrothermal fluids percolating pervasively through the new, still hot, oceanic crust, resulting in amphibole-bearing assemblages (e.g., Kelley and Malpas 1996; Lécuyer and Gruau 1996; Manning and MacLeod 1996; Hart et al. 1999; Boudier et al. 2000; Meurer and Natland 2001; Robinson et al. 2002). Such water is often assumed to be exclusively magmatic (e.g., Tribuzio et al. 2000; Maeda et al. 2002), although seawater contamination as been also advocated (e.g., Gregory and Taylor 1981; Stakes et al. 1991). Primitive MORB melts in mid-ocean ridge environments may contain small but significant amounts of water: from ~0.1–0.2 wt% (for N-and T-MORB; Sobolev and Chaussidon 1996; Dixon et al. 2002) up to ~1.5 wt% (Kamenetsky et al. 2000). If the magma chamber replenishment rate is low, the melt water content may increase during differentiation to amounts, similar to those estimated above. Based on investigations on gabbroic rocks of the Oman ophiolite, Boudier et al. (2000) and Nicolas et al. (2003) concluded that seawater-sourced fluids penetrate even the cumulate crystal mush zone of the magma chambers. We therefore conclude that it is very probable that water-rich fluids are present in high-temperature shear zones.

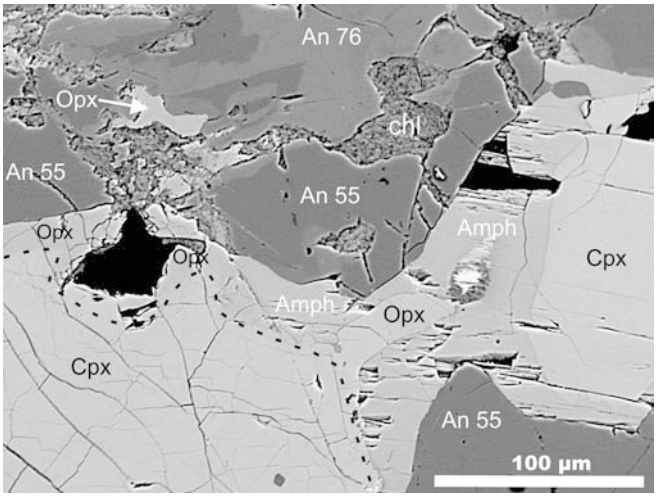

Fig. 10 Backscattered electron image of a high-temperature vein within the gabbro R6a of the Leg 176 (SWIR) showing evidence for hydrous partial melting. Plagioclase at the irregular contact to the vein are markedly enriched in An content (76 mol% An, *light gray*), while the adjacent clinopyroxene has reacted to orthopyroxene and pargasitic amphibole. The *dashed line* marks the reaction zone between clinopyroxene and newly formed orthopyroxene, which is not clearly visible due to very similar gray levels. Away from the high-temperature vein, plagioclase is not affected by the An-enrichment (55 mol% An, *dark gray*). *Cpx* Clinopyroxene; *Opx* orthopyroxene; *Amph* amphibole; An 76, An 55-plagioclase with An content of 76 and 55 mol%, respectively; chl chlorite (alteration product)

Another possibility to initiate hydrous partial melting without excess water is due to the break down of previously existing amphibole-bearing assemblages. Disequilibrium dehydration melting might occur to produce water-saturated melts in small amounts (Wolf and Wyllie 1991). Moreover, hydro-fracturing related to this process could induce and/or promote the high-temperature shearing processes. However, in all products of our low-temperature runs pargasite is the stable amphibole, characterized by high amounts of Na_2O and Al_2O_3. Thus, potential amphiboles for the break down reaction providing a water-rich fluid phase should be of lower thermal stability. Reasonable candidates can be hornblendes, which might be generated during hydrothermal processes at temperatures up to 750 °C (Manning and MacLeod 1996). This implies a re-heating event for the hydrous partial melting, after a stage of cooling and alteration of the deep oceanic crust under sub-solidus conditions, which should result in characteristic textures displaying high-grade prograde metamorphism. This is not observed within typical high-temperatures shear zones of the recent oceanic crust, where shearing proceeds continuously from the magmatic down to the hydrothermal stage passing the brittle/ductile boundary (e.g., Dick et al. 2000). Therefore, we do not believe that dehydration melting plays a role for potential hydrous partial melting within the deep oceanic crust. Instead, we favor a model involving hydrothermal circulation at very high temperatures, in which excess water enters the still very hot, solidified cumulate mush and triggers partial melting.

From consideration of major elements alone, it is difficult to decide whether any given plagiogranite is the formation of late-stage differentiates or generated by partial melting of gabbros. This is shown in the Appendix (Table 4) and in Fig. 7, showing a significant compositional overlap. The low TiO_2 content of our experimental melts is striking, and contrasts with natural plagiogranites. Two processes can conceivably increase the TiO_2 content in a plagiogranitic melt formed by the anatexis of gabbros. Firstly, a mixing with heavy late-stage liquids rich in Ti and Fe residing in the hot, young crust may be possible (unless they are immiscible; e.g., Dixon and Rutherford 1979). The existence of such liquids representing the latest stage of the differentiation of a MORB source has been reported from many locations at mid-oceanic ridge environments (Ludden et al. 1980; Le Roex et al. 1982; Perfit and Fornari 1983; Sinton 1983; Melson and O'Hearn 1986; Juster et al. 1989; Brooks et al. 1991; MacLeod and Yaouancq 2000). That mixing processes

may occur is also suggested by the large variation in major elements of natural plagiogranites, which contrasts with the general compositional uniformity of the major oceanic magmatic rocks generated at mid-ocean ridges (gabbros and MORBs). Secondly, potential protoliths could also include Fe-Ti-rich gabbros (ferrogabbros, oxide gabbros), which would produce partial melts with higher TiO_2 (and FeO) contents (Koepke et al. 2003). At least in slow-spreading ridge systems, innumerable late small intrusions of such gabbros crosscut olivine gabbros, often associated with leucocratic silica-rich rocks (Ozawa et al. 1991; Dick et al. 2000; Natland and Dick 2002).

Briefly summarized, if the temperature estimates in high-temperature shear zones are correct, and provided that a H_2O-bearing fluid phase is present, then partial melting of oceanic gabbros is a viable mechanism for the generation of plagiogranites. It may occur much more often in the oceanic crust than previously expected. However, if melts are really generated this way, their identification would be problematic. Due to the high grade of deformation in high-temperature shear zones, it is likely that melts migrate and/or segregate. During this process, primary generated melts may differentiate and/or may be altered by mixing/mingling processes with highly evolved silica-rich or Fe-Ti-rich late-stage differentiates, eventually in connection with other high-temperature fluids percolating the hot fresh lithosphere. These complex processes would obscure any primary textural or compositional feature.

Only if the melt fraction is high and the grade of local deformation low, would one expect textural features of typical migmatite terrains like the formation of leucosomes and melanosomes to be observable (e.g., the gabbro migmatites of Fuerteventura, Hobson et al. 1998). This is probably the case for ophiolitic plagiogranites which are regarded as products of partial melting (Malpas 1979; Flagler and Spray 1991) and which have textural and compositional (low TiO_2 contents in Fig. 7) characteristics of partial melting products.

Implication for plagiogranite–ferrogabbro associations observed in the oceanic crust

In none of the investigated three systems were Fe-Ti oxides observed as crystallizing phases. This is despite the fact that the redox conditions of the experiments were relatively high (NNO), which would support the stability of magnetite (e.g., Snyder et al. 1993; Toplis and Carroll 1995). The observed instability of oxides in our experiments is attributed to compositional constraints, since our investigated systems are more refractory compared with typical MORB systems. That the saturation temperatures for the Fe-Ti oxides strongly depend on the bulk composition was shown by Snyder et al. (1993). Partial melting of "normal" oceanic gabbros at high water activity under oxidizing conditions thus cannot produce any oxide-rich rocks, since the iron content in the generated melts are generally low (Tables 3 and 4) and oxides are not stable in the experimental crystal assemblage. Thus, the currently observed close association of plagiogranites and ferrogabbros within slow-spreading oceanic crust (e.g., Dick 1998; Shipboard Scientific Party 1999; Natland and Dick 2002; Niu et al. 2002) cannot be regarded as the result of a partial melting event alone. If partial melting in fact occurs, other processes like mixing/mingling of the generated silicic melts with highly differentiated, iron-rich, late-stage liquids is nevertheless required as an explanation for the observed structural and compositional complexity of plagiogranite occurrences within the oceanic crust.

Conclusion

We have produced typical plagiogranitic melts by partial melting of three different oceanic gabbros at temperatures between 900 and 940 °C. The comparison of the compositions of both experimental melts and coexisting crystals with those of natural plagiogranites and of minerals from typical high-temperature microscopic veins implies that partial melting of pre-existing gabbros is a possible model for the generation of plagiogranitic melts within the oceanic crust. This is especially likely at slow spreading ridges like SWIR or MAR, where ductile shearing proceeds at high temperatures up to magmatic conditions, and a fluid rich in water is obviously present, which is manifested in the existence of numerous high-temperature amphibole-bearing veins. As pointed out by Shipboard Scientific Party (1999) such zones in the still hot, just solidified crust are favorable locations for transporting late, highly differentiated liquid (SiO_2-rich and/or Fe-rich) and also for subsequent circulating high-temperature hydrothermal fluids. These zones may have also acted as pathways for later hydrothermal fluids at various temperatures, resulting in the formation of typical hydrothermal minerals.

Acknowledgements Otto Diedrichs's careful sample preparation is gratefully acknowledged. Miriam Haack is thanked for the compilation of the plagiogranite database. Sample 923A from MAR was kindly provided by Laura Gaggero, Genova, Italy. This research used samples provided by the Ocean Drilling Program (ODP). ODP is sponsored by the US National Science Foundation (NSF) and participating countries under management of Joint Oceanographic Institutions (JOI), Inc. The manuscript has been substantially improved after thorough reviews by B. Scaillet and M.B. Wolf. Valuable editorial advice from J. Hoefs is also acknowledged. Funding for this research was provided by grants from the Deutsche Forschungsgemeinschaft (KO 1723/3).

Appendix

Table 4 shows chemical compositions of natural plagiogranites of different tectonic setting and of residual melts of experimental studies used in Figs. 6 and 7.

Table 4 Chemical Compositions of natural plagiogranites of different tectonic setting and of residual melts of experimental studies used in Figs. 6 and 7

Rock type	Setting[a]	Location	n[b]	SiO_2	TiO_2	Al_2O_3	FeO^{tot}	MnO	MgO	CaO	Na_2O	K_2O	H_2O/LOI	P_2O_5	Total[c]	Mg#[d]	Ca#[e]	Reference
Natural plagiogranites of different tectonic setting																		
Volcanic	MOR	Galapagos Rift	(4)	62.06 (1.93)	1.61 (0.41)	12.06 (0.35)	12.09 (0.96)	0.21 (0.03)	1.60 (0.59)	5.82 (0.72)	3.52 (0.54)	0.54 (0.09)		0.34 (0.10)	99.83	21.70	47.72	Fornari
Volcanic	MOR	Galapagos Rift	(4)	66.58 (2.92)	2.44 (0.14)	11.35 (0.26)	10.83 (1.34)	0.05 (0.01)	2.83 (0.29)	0.65 (0.19)	0.80 (0.10)	0.14 (0.04)		0.50 (0.12)	96.16	35.37	31.14	Embley
Volcanic	MOR	MAR	(5)	62.10 (1.71)	1.17 (0.06)	13.37 (0.14)	8.93 (0.36)	0.18 (0.03)	1.62 (0.27)	4.78 (0.51)	3.41 (1.07)	1.09 (0.06)	1.99	0.34 (0.03)	98.97	27.53	43.67	Hekinian
Subvolc.	MOR	MAR	(1)	61.97	0.94	16.00	6.47	0.09	2.43	3.24	5.55	0.75	1.28	0.22	98.94	44.07	24.39	Aumento
Subvolc.	BAB	Southwest Pacific	(7)	65.29 (1.94)	0.84 (0.12)	15.83 (0.84)	4.56 (0.21)	0.17 (0.02)	1.47 (0.49)	3.74 (0.77)	6.12 (0.59)	0.88 (0.10)	1.08 (0.62)	0.20 (0.04)	100.20	40.29	25.23	Nakada
Volcanic	BAB	Lau Basin	(3)	66.90 (1.73)	0.34 (0.02)	11.93 (0.39)	4.90 (0.19)	0.10 (0.00)	1.31 (0.10)	4.26 (0.19)	4.96 (0.67)	0.77 (0.02)	3.65 (1.73)	0.12 (0.01)	99.25	35.91	32.19	Falloon
Volcanic	BAB	Pacific	(6)	60.70 (0.25)	1.28 (0.04)	12.64 (0.13)	11.75 (0.26)		1.31 (0.04)	5.44 (0.03)	4.27 (0.06)	0.51 (0.01)		0.27 (0.01)	98.16	18.93	41.32	Bloomer
Plutonic	SSZ-O	California	(15)	66.69 (2.12)	0.80 (0.18)	15.14 (0.57)	5.37 (1.41)	0.11 (0.05)	1.63 (0.43)	4.90 (0.92)	4.86 (0.73)	0.29 (0.24)	0.99 (0.76)	0.20 (0.10)	100.99	38.94	35.78	Beard
Plutonic	SSZ-O	Greece	(1)	67.79	0.48	15.71	*2.87*	0.04	0.21	6.45	5.34	0.30	0.70	0.09	99.98	13.30	40.03	Tsikouras
Plutonic	SSZ-O	Norway	(6)	64.93 (3.28)	0.84 (0.40)	15.20 (0.93)	5.82 (1.64)	0.07 (0.03)	1.68 (0.79)	5.97 (1.49)	4.87 (0.71)	0.20 (0.08)	0.62 (0.46)	0.24 (0.10)	100.42	37.70	40.38	Pedersen
Plutonic	SSZ-O	Newfound-land	(4)	60.25 (1.68)	0.54 (0.22)	18.05 (0.69)	2.47 (1.04)	0.03 (0.00)	1.49 (0.65)	5.71 (1.63)	8.26 (0.34)	0.05 (0.04)	2.54 (0.82)	0.17 (0.11)	99.54	55.78	27.66	Malpas
Plutonic	SSZ-O	Oregon	(1)	65.65	0.62	14.46	*5.79*	0.12	1.91	5.76	2.98	0.53	1.21	0.10	99.13	40.89	51.65	Phelps
Plutonic	SSZ-O	Greece	(1)	68.13	0.31	10.40	*3.19*	0.10	0.76	7.90	4.12	0.01	4.34		99.26	33.35	51.45	Bébien
Plutonic	SSZ-O	Chile	(3)	65.51 (1.59)	0.81 (0.34)	13.64 (2.57)	5.89 (1.92)	0.11 (0.05)	1.46 (0.63)	6.28 (0.64)	1.99 (0.49)	0.67 (1.15)	2.60 (1.04)	0.17 (0.03)	99.12	34.25	63.58	Saunders
Plutonic	SSZ-O	Washington	(6)	66.13 (2.41)	0.30 (0.05)	14.12 (0.74)	4.88 (1.10)	0.11 (0.05)	2.66 (1.47)	4.75 (1.41)	4.25 (0.31)	0.56 (0.22)			97.74	53.33	38.18	Brown
Plutonic	SSZ-O	Crete	(2)	64.50 (4.53)	0.49 (0.19)	15.65 (0.78)	6.85 (1.63)	0.15 (0.04)	1.95 (1.41)	5.70 (0.60)	2.80 (0.18)	0.67 (0.03)	1.40 (0.28)	0.06 (0.02)	100.19	37.33	52.96	Koepke
Plutonic	MOR	SWIR Leg 176	(17)	61.00 (2.79)	0.64 (0.39)	16.72 (1.71)	3.90 (1.64)	0.08 (0.04)	3.49 (1.88)	6.09 (2.65)	6.73 (1.62)	0.21 (0.14)		0.10 (0.24)	98.95	65.20	33.33	Niu
Anatectic	SSZ-O	Newfound-land	(4)	68.53 (0.95)	0.25 (0.07)	14.55 (0.56)	3.48 (0.73)	0.08 (0.01)	1.23 (0.25)	2.90 (1.05)	4.73 (0.61)	0.87 (0.28)	1.91 (0.17)	0.08 (0.05)	98.60	42.53	25.30	Malpas
Anatectic	SSZ-O	Canada	(1)	59.86	0.26	19.69	*3.29*	0.07	1.98	6.48	6.90	0.14	1.99	0.19	100.85	55.77	34.17	Flagler
Residual melts of experimental runs																		
Protolith: gabbro, 940 °C[f]			(3)	60.92 (0.35)	0.36 (0.19)	20.09 (0.74)	4.87 (0.90)	0.11 (0.04)	2.87 (0.51)	6.36 (0.78)	3.98 (0.37)	0.30 (0.05)		0.13 (0.09)	100.00	55.24	46.89	This study
Protolith: gabbro, 900 °C[f]			(3)	65.56 (2.60)	0.12 (0.02)	19.21 (2.91)	3.83 (0.63)	0.08 (0.04)	2.13 (0.23)	5.36 (0.24)	3.06 (0.35)	0.41 (0.27)		0.24 (0.14)	100.00	53.80	49.19	This study
Protolith: MORB, 955 °C[g]			(1)	67.64	1.25	15.41	6.26	0.08	1.29	3.98	3.24	0.31		0.54	100.00	30.23	40.47	Spulber
Hydrous MORB, 950 °C[h]			(1)	61.33	1.17	17.98	7.49	0.1	1.84	4.98	4.67	0.18		0.26	100.00	34.00	37.08	Berndt

[a]Tectonic settings: *MOR* Mid-ocean ridge; *BAB* back-arc basin; *SSZ-O* supra-subduction zone ophiolite
[b]Number of analyses; the number in parentheses below each average corresponds to the standard deviation
[c]The analyses of the experimental melts were normalized to 100%
[d]Mg# = molar $100 \times MgO/(MgO + FeO^{tot})$
[e]Ca# = molar $100 \times CaO/(CaO + NaO_{0.5})$
[f]Partial melting experiments using oceanic gabbros as starting material; average of three different gabbros (this study)

[g]Partial melting experiments using a natural primitive MORB as starting material (run #74A, pressure 100 MPa, T = 955 °C, G-CH buffer)
[h]Crystallization experiments with a primitive, hydrous MORB glass (run#151, pressure 200 MPa, T = 950 °C, QFM buffer, water saturated)
Only plagiogranites with SiO_2 contents varying between 60 and 70 wt% were considered, to facilitate comparisons with our experimental data
References: Analyses of volcanic rocks (except data of Bloomer) are obtained from the PETDB data base of Lamont-Doherty Earth Observatory of Columbia University (Lehnert et al. 2000): Aumento (1969), Embley et al. (1988), Falloon et al. (1992), Fornari et al. (1983), Hekinian et al. (1997), Nakada et al. (1994); data of Bloomer are obtained from the Smithsonian Institution Volcanic Glass Individual Analysis File (VG no# 9772–9777, available at http://www.nmnh.si.edu/minsci/research/glass/g3_table1.txt. Analyses from ophiolites: Beard (1998), Bébien (1991), Brown et al. (1979), Flagler and Spray (1991), Koepke (1986), Malpas (1979), Pedersen and Malpas (1984), Phelps and Avé Lallemant (1980), Saunders et al. (1979), Tsikouras and Hatzipanagiotou (1998). Analyses from Leg 176: Niu et al. (2002). Analyses from experimental paper: Berndt (2002), Dixon-Spulber and Rutherford (1983)

References

Aldiss DT (1981) Plagiogranites from the ocean crust and ophiolites. Nature 289:577–578

Amri I, Benoit M, Ceuleneer G (1996) Tectonic setting for the genesis of oceanic plagiogranites: evidence from a paleospreading structure in the Oman ophiolite. Earth Planet Sci Lett 139:177–194

Aumento F (1969) Diorites from the Mid-Atlantic Ridge at 45 degree N. Science 165:1112–1113

Barker F (1979) Trondhjemites, dacites and related rocks. Elsevier, Amsterdam, 659 pp

Beard JS (1998) Polygenetic tonalite-trondhjemite-granodiorite (TTG) magmatism in the Smartville Complex, northern California with a note on LILE depletion in plagiogranites. Mineral Petrol 64:15–45

Beard JS, Lofgren GE (1991) Dehydration melting and water-saturated melting of basaltic and andesitic greenstones and amphibolites at 1, 3, and 6.9 kb. J Petrol 32:365–401

Bébien J (1991) Enclaves in plagiogranites of the Guevgueli ophiolitic complex, Macedonia, Greece. In: Didier J, Barbarin B (eds) Enclaves and granite petrology, developments in petrology, vol 13. Elsevier, Amsterdam, pp 205–219

Bédard JH (1991) Cumulate recycling and crustal evolution in the Bay of Islands ophiolite. J Geol 99:225–249

Berndt J (2002) Differentiation of MOR Basalt at 200 MPa: Experimental techniques and influence of H_2O and fO_2 on phase relations and liquid line of descent. PhD Thesis, Universitaet Hannover, 118 pp

Berndt J, Holtz F, Koepke J (2001) Experimental constraints on storage conditions in the chemically zoned phonolitic magma chamber of the Laacher See volcano. Contrib Mineral Petrol 140:469–486

Berndt J, Liebske C, Holtz F, Freise M, Nowak M, Ziegenbein D, Hurkuck D, Koepke J (2002) A combined rapid-quench and H_2-membrane setup for internally heated pressure vessels: Description and application for water solubility in basaltic melts. Am Mineral 87:1717–1726

Blundy J, Holland TJB (1990) Calcic amphibole equilibria and a new amphibole-plagioclase geothermometer. Contrib Mineral Petrol 104:208–224

Boudier F, Godard M, Armbruster C (2000) Significance of gabbronorite occurrence in the crustal section of the Semail ophiolite. Mar Geophys Res 21:307–326

Brooks CK, Larsen LM, Nielsen TFD (1991) Importance of iron-rich tholeiitic magmas at divergent plate margins: a reappraisal. Geology 19:269–272

Brown EH, Bradshaw JY, Mustoe GE (1979) Plagiogranite and keratophyre in ophiolite Fidalgo Island, Washington. Geol Soc Am Bull, Part I 90:493–507

Carmichael ISE, Turner FJ, Verhoogen J (1974) Igneous petrology. University of California, Berkeley, 739 pp

Casey JF (1997) Comparison of major- and trace-element geochemistry of abyssal peridotites and mafic plutonic rocks with basalts from the MARK region of the Mid-Atlantic Ridge. In: Karson JA, Cannat M, Miller DJ, Elthon D (eds) Proc ODP, Sci Results 153. Ocean Drilling Program, College Station, TX, pp 181–241

Christie DM, Carmichael ISE, Langmuir CH (1986) Oxidation states of mid-ocean ridge basalt glasses. Earth Planet Sci Lett 79:397–411

Coleman RG (1977) Ophiolites. Springer, Berlin Heidelberg New York, 229 pp

Coleman RG, Donato MM (1979) Oceanic plagiogranite revisited. In: Barker F (ed) Trondhjemites, dacites, and related rocks. Elsevier, Amsterdam, pp 149–167

Cortesogno L, Gaggero L, Zanetti A (2000) Rare earth and trace elements in igneous and high-temperature metamorphic minerals of oceanic gabbros (MARK area, Mid-Atlantic Ridge). Contrib Mineral Petrol 139:373–393

Dick HJB (1998) Indian ocean's Atlantis Bank yields deep-earth insight. Oceanus 41:29–32
Dick HJB, Natland JH, Alt JC, Bach W, Bideau D, Gee JS, Haggas S, Hertogen JGH, Hirth G, Holm PM, Ildefonse B, Iturrino GJ, John BE, Kelley DS, Kikawa E, Kingdon A, LeRoux PJ, Maeda J, Meyer PS, Miller DJ, Naslund HR, Niu YL, Robinson PT, Snow J, Stephen RA, Trimby PW, Worm HU, Yoshinobu A (2000) A long in situ section of the lower ocean crust: results of ODP Leg 176 drilling at the Southwest Indian Ridge. Earth Planet Sci Lett 179:31–51
Dixon JE, Leist L, Langmuir CH, Schilling J (2002) Recycled dehydrated lithosphere observed in plume-influenced mid-ocean-ridge basalt. Nature 420:385–389
Dixon S, Rutherford MJ (1979) Plagiogranites as late-stage immiscible liquids in ophiolite and mid-oceanic ridge suites: an experimental study. Earth Planet Sci Lett 45:45–60
Dixon-Spulber S, Rutherford MJ (1983) The origin of rhyolite and plagiogranite in oceanic crust: an experimental study. J Petrol 24:1–25
Embley RW, Jonasson IR, Perfit MR, Franklin JM, Tivey MA, Malahoff A, Smith MF, Francis TJG (1988) Submersible investigations of an extinct hydrothermal system on the Galapagos Ridge: Sulfide mound, stockwork zone, and differentiated lavas. Can Mineral 26:517–539
Ernst WG, Liou J (1998) Experimental phase-equilibrium study of Al- and Ti-contents of calcic amphibole in MORB—a semi-quantitative thermobarometer. Am Mineral 83:952–969
Falloon TJ, Malahoff A, Zonenshain LP, Bogdanov Y (1992) Petrology and geochemistry of back-arc basin basalts from Lau Basin spreading ridges at 15 degree, 18 degree and 19 degree S. Mineral Petrol 47:1–35
Flagler PA, Spray JG (1991) Generation of plagiogranite by amphibolite anatexis in oceanic shear zones. Geology 19:70–73
Floyd PA, Yaliniz MK, Goncuoglu MC (1998) Geochemistry and petrogenesis of intrusive and extrusive ophiolitic plagiogranites, Central Anatolian Crystalline Complex, Turkey. Lithos 42:225–241
Fornari DJ, Perfit MR, Malahoff A, Embley RU (1983) Geochemical studies of abyssal lavas recovered by DSRV Alvin from Eastern Galapagos Rift, Inca Transform, and Ecuador Rift. 1. Major element variations in natural glasses and spatial distribution of lavas. J Geophys Res 88:10519–10529
Früh-Green GL, Plas A, Dell'Angelo LN (1996) Mineralogic and stable isotope record of polyphase alteration of upper crustal gabbros of the pacific rise (Hess Deep, Site 894). In: Mével C, Gillis KM, Allan JF, Meyer PS (eds) Proc ODP, Sci Results 147. Ocean Drilling Program, College Station, TX, pp 235–254
Gaggero L, Cortesogno L (1997) Metamorphic evolution of oceanic gabbros: recrystallization from subsolidus to hydrothermal conditions in the MARK area (ODP Leg 153). Lithos 40:105–131
Gerlach DC, Leeman WP, Avé Lallemant HG (1981) Petrology and geochemistry of plagiogranite in the Canyon Mountain ophiolite, Oregon. Contrib Mineral Petrol 72:82–92
Gregory RT, Taylor HP (1981) An oxygen isotope profile in a section of Cretaceous oceanic crust, Semail ophiolite, Oman: evidence for $d^{18}O$ buffering of the ocean by deep (>5 km) seawater hydrothermal circulation at Mid-Ocean Ridges. J Geophys Res 86:2737–2755
Hacker BR (1990) Amphibolite-facies to granulite-facies reactions in experimentally deformed, unpowdered amphibolite. Am Mineral 75:1349–1361
Hart SR, Blusztajn J, Dick HJB, Meyer PS, Muehlenbachs K (1999) The fingerprint of seawater circulation in a 500-meter section of ocean crust gabbros. Geochim Cosmochim Acta 63:4059–4080
Hébert R, Constantin M, Robinson PT (1991) Primary mineralogy of Leg 118 gabbroic rocks and their place in the spectrum of oceanic mafic igneous rocks. In: Von Herzen RP, Robinson PT et al. (eds) Proc ODP, Sci Results 118. Ocean Drilling Program, College Station, pp 3–20
Hekinian R, Stoffers P, Devey CW, Ackermand D, Hemond C, O'Connor J, Bihard N, Maia M (1997) Intraplate versus ridge volcanism on the Pacific-Antarctic Ridge near 37 degree S–111 degree W. J Geophys Res 102:12265–12286
Helz RT (1973) Phase relations of basalt in their melting ranges at $P_{H_2O} = 5$ kb as a function of oxygen fugacity. J Petrol 14:249–302
Helz RT (1976) Phase relations of basalt in their melting ranges at $P_{H_2O} = 5$ kb. Part II: melt compositions. J Petrol 17:139–193
Hobson A, Bussy F, Hernandez J (1998) Shallow-level migmatisation of gabbros in a metamorphic contact aureole, Fuerteventura Basal Complex, Canary Islands. J Petrol 39:1025–1037
Holloway JR, Burnham CW (1972) Melting relations of basalt with equilibrium water pressure less than total pressure. J Petrol 13:1–29
Irvine TN, Baragar WRA (1971) A guide to the chemical classification of the common volcanic rocks. Can J Earth Sci 8:532–548
Johannes W, Holtz F (1996) Petrogenesis and experimental petrology of granitic rocks. Minerals and rocks, vol 22. Springer, Berlin Heidelberg New York, 335 pp
Johannes W, Koepke J (2001) Uncomplete reaction of plagioclase in experimental dehydration melting of amphibolite. Aust J Earth Sci 48:581–590
Johannes W, Koepke J, Behrens H (1994) Partial melting reactions of plagioclases and plagioclase-bearing systems. In: Parson I (ed) Feldspars and their reactions, NATO ASI Series, vol 421. Kluwer, Dordrecht, pp 161–194
Johnson MC, Anderson AT, Rutherford MJ (1994) Pre-eruptive volatile contents of magmas. In: Carroll MR, Holloway JR (eds) Volatiles in magmas. Rev Mineral, vol. 30. Mineralogical Society of America, Washington, DC, pp 281–330
Juster TC, Grove TL, Perfit MR (1989) Experimental constraints on the generation of Fe-Ti basalts, andesites, and rhyodacites at the Galapagos spreading centre, 85°W and 95°W. J Geophys Res 94:9251–9274
Kamenetsky VS, Everard JL, Crawford AJ, Varne R, Eggins SM, Lanyon R (2000) Enriched end-member of primitive MORB melts: petrology and geochemistry of glasses from Macquarie Island (SW Pacific). J Petrol 41:411–430
Kawamoto T (1996) Experimental constraints on differentiation and H_2O abundance of calc-alkaline magmas. Earth Planet Sci Lett 144:577–589
Kelley DS, Malpas J (1996) Melt-fluid evolution in gabbroic rocks from Hess Deep. In: Mével C, Gillis KM, Allan JF, Meyer PS (eds) Proc ODP, Sci Results 147. Ocean Drilling Program, College Station, TX, pp 213–226
Koepke J (1986) Die Ophiolithe der südägäischen Inselbrücke. PhD Thesis, Technische Universitaet Braunschweig, 204 pp
Koepke J, Berndt J, Bussy F (2003) An experimental study on the shallow-level migmatization of ferrogabbros from the Fuerteventura Basal Complex, Canary Islands. Lithos 69:105–125
Koepke J, Seidel E, Kreuzer H (2002) Ophiolites on the Southern Aegean islands Crete, Karpathos and Rhodes: composition, geochronology and position within the ophiolite belts of the Eastern Mediterranean. Lithos 65:183–203
Le Maitre RW (1989) A classification of the igneous rocks and glossary of terms. Blackwell, Oxford, 193 pp
Le Roex AP, Dick HJB, Reid AM, Erlank AJ (1982) Ferrobasalts from the Spiess Ridge segment of the southwest Indian Ridge. Earth Planet Sci Lett 60:437–451
Leake BE, Woolley AR, Birch WD, Gilbert MC, Grice JD, Hawthorne FC, Kato A, Kisch HJ, Krivovichev VG, Linthout K, Laird J, Mandarino J, Maresch WV, Nickel EH, Rock NMS, Schumacher JC, Smith DC, Stephenson NCN, Ungaretti L, Whittaker EJW, Youzhi G (1997) Nomenclature of amphiboles—report of the subcommittee on amphiboles of the International Mineralogical Association Commission on new minerals and mineral names. Eur J Mineral 9:623–651
Lécuyer C, Gruau G (1996) Oxygen and strontium isotope compositions of Hess Deep gabbros (Holes 894F and 894G): high-temperature interaction of sea-water with the oceanic crust

layer 3. In: Mével C, Gillis KM, Allan JF, Meyer PS (eds) Proc ODP, Sci Results 147. Ocean Drilling Program, College Station, TX, pp 227–234
Lehnert K, Su Y, Langmuir CH, Sarbas B, Nohl U (2000) A global geochemical database structure for rocks. Geochem Geophys Geosyst 1:1999GC000026
Ludden JN, Thompson G, Bryan WB, Frey FA (1980) The origin of lavas from the Ninetyeast Ridge, Eastern Indian Ocean: an evaluation of fractional crystallization models. J Geophys Res 85:4405–4420
MacLeod CJ, Yaouancq G (2000) A fossil melt lens in the Oman ophiolite: implications for magma chamber processes at fast spreading ridges. Earth Planet Sci Lett 176:357–373
Maeda J, Naslund HR, Jang YD, Kikawa E, Tajima T, Blackburn WH (2002) High-temperature fluid migration within oceanic Layer 3 gabbros, Hole 735B, Southwest Indian Ridge: implications for the magmatic-hydrothermal transition at slowspreading mid-ocean ridges. In: Natland JH, Dick HJB, Miller DJ, Von Herzen RP (eds) Proc ODP, Sci Results 176. Ocean Drilling Program, College Station, TX, pp 1–56, [Online] http://www-odp.tamu.edu/publications/176_SR/VOLUME/CHAPTERS/SR176_04.PDF > [Cited 23-08-2003]
Malpas J (1979) Two contrasting trondhjemite associations from transported ophiolites in Western Newfoundland: Initial report. In: Barker F (ed) Trondhjemites, dacites, and related rocks. Elsevier, Amsterdam, pp 465–487
Manning CE, MacLeod CJ (1996) Fracture-controlled metamorphism of Hess Deep gabbros, Site 894: constraints on the roots of mid-ocean-ridge hydrothermal systems at fast-spreading centers. In: Mével C, Gillis KM, Allan JF, Meyer PS (eds) Proc ODP, Sci Results 147. Ocean Drilling Program, College Station, TX, pp 189–212
Martel C, Pichavant M, Bourdier JL, Traineau H, Holtz F, Scaillet B (1998) Magma storage conditions and control of eruption regime in silicic volcanoes; experimental evidence from Mt. Pelee. Earth Planet Sci Lett 156:89–99
Melson WG, O'Hearn T (1986) ''Zero-age'' variations in the composition of abyssal volcanic rocks along the axial zone of the Mid-Atlantic Ridge. In: Vogt PR, Tucholke BE (eds) The geology of North America. Geological Society of America, pp 117–136
Merzbacher C, Eggler DH (1984) A magmatic geohygrometer: application to Mount St. Helens and other dacitic magmas. Geology 12:587–590
Meurer WP, Natland JH (2001) Apatite compositions from oceanic cumulates with implications for the evolution of mid-ocean ridge magmatic systems. J Volcanol Geotherm Res 110:281–298
Mével C (1988) Metamorphism in ocean layer 3, Gorringe Bank, Eastern Atlantic. Contrib Mineral Petrol 100:496–509
Miyashiro A (1974) Volcanic rock series in island arcs and active continental margins. Am J Sci 274:321–355
Nakada S, Maillet P, Monjaret MC, Fujinawa A, Urabe T (1994) High-Na dacite from the Jean Charcot Trough (Vanuatu), Southwest Pacific. Mar Geol 116:197–213
Natland JH, Dick HJB (2002) Formation of the lower ocean crust and the crystallization of gabbroic cumulates at a very slowly spreading ridge. J Volcanol Geotherm Res 110:191–233
Nicolas A (1989) Structures of ophiolites and dynamics of oceanic lithosphere. Kluwer, Dordrecht, 376 pp
Nicolas A, Mainprice D, Boudier F (2003) High-temperature seawater circulation throughout crust of oceanic ridges: a model derived from the Oman ophiolite. J Geophys Res 108, No B8, 2371
Niu Y, Gilmore T, Mackie S, Greig A, Bach W (2002) Mineral chemistry, whole-rock compositions, and petrogenesis of Leg 176 gabbros: data and discussion. In: Natland JH, Dick HJB, Miller DJ, Von Herzen RP (eds) Proc ODP, Sci Results 176. Ocean Drilling Program, College Station, TX, pp 1–60, [Online] http://www-odp.tamu.edu/publications/176_SR/VOLUME/CHAPTERS/SR176_08.PDF [Cited 23-08-2003]
Ozawa K, Meyer PS, Bloomer SH (1991) Mineralogy and textures of iron-titanium-oxide gabbros from hole 735B. In: Von Herzen RP, Robinson PT et al (eds) Proc ODP, Sci Results 118. Ocean Drilling Program, College Station, TX, pp 41–73
Panjasawatwong Y, Danyushevsky LV, Crawford AJ, Harris KL (1995) An experimental study of the effects of melt composition on plagioclase—melt equilibria at 5 and 10 kbar: implications for the origin of magmatic high-An plagioclase. Contrib Mineral Petrol 118:420–432
Patino Douce AE, Beard JS (1995) Dehydration-melting of biotite gneiss and quartz amphibolite from 3 to 15 kbar. J Petrol 36:707–738
Pedersen RB, Malpas J (1984) The origin of oceanic plagiogranites from the Karmoy ophiolite, Western Norway. Contrib Mineral Petrol 88:36–52
Perfit MR, Fornari DJ (1983) Geochemical studies of abyssal lavas recovered by DSRV Alvin from Eastern Galapagos Rift, Inca Transform, and Ecuador Rift: 2. Phase chemistry and crystallization history. J Geophys Res 88, B12:10530–10550
Phelps D, Avé Lallemant HG (1980) The Sparta ophiolite complex, northeast Oregon: a plutonic equivalent to low K_2O island-arc volcanism. Am J Sci 280-A:345–358
Pouchou JL, Pichoir F (1991) Quantitative analysis of homogeneous or stratified microvolumes applying the model ''PAP''. In: Heinrich KFJ, Newbury DE (eds) Electron probe quantification. Plenum Press, New York, pp 31–75
Rapp RP, Watson EB (1995) Dehydration melting of metabasalt at 8–32 kbar: implications for continental growth and crust-mantle recycling. J Petrol 36:891–931
Rapp RP, Watson EB, Miller CF (1991) Partial melting of amphibolite/eclogite and the origin of Archean trondhjemites and tonalites. Precambrian Res 51:1–25
Robinson PT, Erzinger J, Emmermann R (2002) The composition and origin of igneous and hydrothermal veins in the lower ocean crust—ODP Hole 735B, Southwest Indian Ridge. In: Natland JH, Dick HJB, Miller DJ, Von Herzen RP (eds) Proc ODP, Sci Results 176. Ocean Drilling Program, College Station, TX, pp 1–66, [Online] http://www-odp.tamu.edu/publications/176_SR/VOLUME/CHAPTERS/SR176_09.PDF [Cited 23-08-2003]
Rushmer T (1991) Partial melting of two amphibolites: contrasting experimental results under fluid-absent conditions. Contrib Mineral Petrol 107:41–59
Rushmer T (1993) Experimental high-pressure granulites: some applications to natural mafic xenolith suites and Archean granulite terranes. Geology 21:411–414
Saunders AD, Tarney J, Stern CR, Dalziel IWD (1979) Geochemistry of mesozoic marginal basin floor igneous rocks from southern Chile. Geol Soc Am Bull, Part I 90:237–258
Scaillet B, Evans WB (1999) The 15. June 1991 eruption of Mount Pinatubo. 1. Phase equilibra and pre-eruption P–T–fO_2–fH_2O conditions of the dacite magma. J Petrol 3:381–411
Scaillet B, Pichavant M, Roux J (1995) Experimental crystallization of leucogranite magmas. J Petrol 36:663–705
Seifert K, Gibson I, Weis D, Brunotte D (1996) Geochemistry of metamorphosed cumulate gabbros from Hole 900, Iberia Abyssal Plain. In: Whitmarsh RB, Sawyer DS, Klaus A, Masson DG (eds) Proc ODP, Sci Results 149. Ocean Drilling Program, College Station, TX, pp 471–488
Sen C, Dunn T (1994) Dehydration melting of a basaltic composition amphibolite at 1.5 and 2.0 GPa: implications for the origin of adakites. Contrib Mineral Petrol 117:394–409
Shi P (1993) Low-pressure phase relationships in the system Na_2O-CaO-FeO-MgO-Al_2O_3-SiO_2 at 1,100 °C, with implications for the differentation of basaltic magmas. J Petrol 34:743–762
Shipboard Scientific Party (1999) Site 735. In: Dick HJB, Natland JH, Miller DJ (eds) Proc ODP, Init Repts 176. Ocean Drilling Program, College Station, TX, pp 1–314, [Online] http://www-odp.tamu.edu/publications/176_IR/VOLUME/CHAPTERS/CHAP_03.PDF[Cited 23-08-2003]

Sinton JM, Wilson DS, Christie DM, Hey RN, Delaney JR (1983) Petrologic consequences of rift propagating on oceanic spreading ridges. Earth Planet Sci Lett 62:193–207

Sisson TW, Grove TL (1993) Experimental investigations of the role of H_2O in calc-alkaline differentiation and subduction zone magmatism. Contrib Mineral Petrol 113:143–166

Snyder D, Carmichael ISE, Wiebe RA (1993) Experimental study of liquid evolution in an Fe-rich, layered mafic intrusion: constraints of Fe-Ti oxide precipitation on the T- fO_2 and T-p paths of tholeiitic magmas. Contrib Mineral Petrol 113:73–86

Sobolev AV, Chaussidon M (1996) H_2O concentration in primary melts from supra-subduction zones and mid-ocean ridges: Implication for H_2O storage and recycling in the mantle. Earth Planet Sci Lett 137:45–55

Spray JG, Dunning GR (1991) A U/Pb age for the Shetland Islands oceanic fragment, Scottish Caledonides: evidence from anatectic plagiogranites in 'layer 3' shear zones. Geol Mag 128:667–671

Stakes D, Mével C, Cannat M, Chaput T (1991) Metamorphic stratigraphy of hole 735B. In: Von Herzen RP, Robinson PT et al (eds) Proc ODP, Sci Results 118. Ocean Drilling Program, College Station, TX, pp 153–180

Thayer TP (1977) Some implications of sheeted dike swarms in ophiolitic complexes. Geotectonics 11:419–426

Thy P, Lofgren GE (1994) Experimental constraints on the low-pressure evolution of transitional and mildly alkalic basalts: the effect of Fe-Ti oxide minerals and the origin of basaltic andesites. Contrib Mineral Petrol 116:340–351

Toplis MJ, Carroll MR (1995) An experimental study of the influence of oxygen fugacity on Fe-Ti oxide stability, phase relations, and mineral-melt equilibra in ferro-basaltic systems. J Petrol 36:1137–1170

Tribuzio R, Tiepelo M, Thirlwall MF (2000) Origin of titanian pargasite in gabbroic rocks from the Northern Apennine ophiolites (Italy): Insight into the late-magmatic evolution of a MOR-type intrusive sequence. Earth Planet Sci Lett 176:281–293

Tsikouras B, Hatzipanagiotou K (1998) Plagiogranite and leucogranite relationships in an ophiolite on the Thethys Ocean (Samothraki, N. Aegean, Greece). Neues Jahrb Miner Monatsh 1:13–35

Turner FJ, Verhoogen J (1960) Igneous and metamorphic petrology. McGraw-Hill , New York, 694 pp

Wolf MB, Wyllie PJ (1991) Dehydration-melting of solid amphibolite at 10 kbar—textural development, liquid interconnectivity and applications to the segregation of magmas. Mineral Petrol 44:151–179

Wolf MB, Wyllie PJ (1994) Dehydration-melting of amphibolite at 10 kbar: the effects of temperature and time. Contrib Mineral Petrol 115:369–383